10 Hz GPS seismology for moderate magnitude earthquakes: the case of the Mw 6.3 L'Aquila (Central Italy) event

A. Avallone,[1] M. Marzario,[1] A. Cirella,[2] A. Piatanesi,[2] A. Rovelli,[2] C. Di Alessandro,[3] E. D'Anastasio,[1] N. D'Agostino,[1] R. Giuliani,[4] and M. Mattone[4].

[1]A. Avallone, M. Marzario, E. D'Anastasio, N. D'Agostino, Istituto Nazionale di Geofisica e Vulcanologia, Centro Nazionale Terremoti, Via di Vigna Murata 605, I-00143, Roma, Italy.

[2]A. Cirella, A. Piatanesi, A. Rovelli, Istituto Nazionale di Geofisica e Vulcanologia, sezione di Roma1, Via di Vigna Murata 605, I-00143, Roma, Italy.

[3]C. Di Alessandro, Pacific Earthquake Engineering Research Center (PEER), University of California, Berkeley, 325 Davis Hall, Mail Code 1792, Berkeley, CA 94720-1792, USA.

[4]R. Giuliani, M. Mattone, Dipartimento della Protezione Civile, Ufficio Rischio Sismico, Via Vitorchiano 4, I-00189, Roma, Italy.

Abstract

The 2009 April 6th Mw 6.3 L'Aquila destructive earthquake was successfully recorded by closely spaced 10-Hz and 1-Hz recording GPS receivers and strong motion accelerometers located above or close to the 50° dipping activated fault. We retrieved both static and dynamic displacements from Very High-Rate GPS (VHRGPS) recordings by using Precise Point Positioning kinematic analysis. We compared the GPS positions time series with the closest displacement time series obtained by doubly-integrating strong motion data, first, to assess the GPS capability to detect the first seismic arrivals (P waves) and, secondly, to evaluate the accelerometers capability to detect co-seismic offsets up to ~45 s after the earthquake occurrence. By comparing seismic and VHRGPS frequency contents, we inferred that GPS sampling rates greater than 2.5 Hz (i.e. 5 or 10 Hz) are required in the near-field of moderate magnitude events to provide "alias-free" solutions of coseismic dynamic displacements. Finally, we assessed the consistency of the dynamic VHRGPS results as a constraint on the kinematic rupture history of the mainshock. These results suggested that the high-rate sampling GPS sites in the near field can be as useful as strong motion station for earthquake source studies.

1. Introduction

[1] The use of Global Positioning System (GPS) has been traditionally used to study the long term deformation field occurring at regional [*McClusky et al.*, 2000; *Dragert et al.*, 2001; *Melbourne and Webb*, 2002; *Larson et al.*, 2004] or global [*Dixon et al.*, 1991*; Argus and Heflin*, 1995*; Larson et al.*, 1997] scales through the analysis of position time series of daily solutions. The developments of both GPS instrumentation and data storage capabilities have increased the sensitivity of GPS receivers to behave as seismometers for large-magnitude events, by decreasing the sampling

interval of the data acquisition and by processing the data with a kinematic approach, that means a solution for each epoch [*Larson et al.*, 2003]. Although high-frequency GPS measurements of dynamic displacements are several orders of magnitude less sensitive than the seismometers readings, they do not suffer from drift, clipping or instrument tilting. The dynamic displacements of several earthquakes have been captured at regional and teleseismic distances. It has proven that the 30-s-rated epoch by epoch solution is enough to determine instantaneous geodetic positions [*Bock et al.*, 2000] and rapid estimations of magnitude [*Blewitt et al.*, 2006]. Other investigations have demonstrated the utility of 1 Hz data to detect seismic waves in good agreement with seismic data [*Larson et al.*, 2003; *Bock et al.*, 2004; *Wang et al.*, 2007; *Emore et al.*, 2007] and to model fault slip [*Ji et al.*, 2004; *Miyazaki et al.*,2004; *Davis and Smalley*, 2009; *Yokota et al.*, 2009]. However, *Smalley* [2009] showed that 1-Hz GPS recordings of coseismic displacements at very small epicentral distances from M 6 earthquakes are aliased, and that 5-Hz recordings for M 7 (or larger) events may also be aliased. Thus, a higher temporal and spatial resolution is needed to produce alias-free recordings of coseismic displacements, in particular for low to moderate magnitude earthquakes ($5 < M < 7$).

[2] The 2009 April 6th L'Aquila earthquake struck the Abruzzi region with a magnitude (Mw 6.3) which falls into the typical moderate magnitude range that can occur on the active normal faults documented in the Apennines [*Boncio et al.*, 2004; *Roberts and Michetti*, 2004; *Galli et al.*, 2008; fig. 1]. This earthquake occurred on the Paganica fault [*Emergeo Working Group* 2009; *Falcucci et al.* 2009; fig.1] and it was recorded by a number of 1-Hz CGPS sites belonging to the Rete Integrata Nazionale GPS (RING, http://ring.gm.ingv.it) and to other regional networks [*D'Agostino et al.*, 2008]. The closest 1-Hz CGPS sites are INGP (RING) and INFN (DPC, http://www.protezionecivile.it), respectively 6.5 km and 13.8 km from the epicenter [*Chiarabba et al.*, 2009]. A few survey-style GPS benchmarks were also installed a few days before the

68 mainshock [*Anzidei et al.*, 2009]. In two of these GPS sites, ROIO (Poggio di Roio) and CADO
69 (Fossa), respectively 2.3 km and 10.4 km from the epicenter, a Leica AX1202 antenna was installed
70 on a 1.5 m tall concrete pillar and the receiver (Leica GX1230) was set up with a 10 Hz sampling
71 interval. No GPS sites outside the epicentral area were recording with the same sampling rate.

72 [3] Recent studies focusing on the L'Aquila event GPS coseismic offsets [*Anzidei et al.*, 2009] as
73 well as the GPS–derived initial post-seismic deformation [*Cheloni et al.*, 2010] have been carried
74 out using daily network solutions. In our work, we will focus on the description of both the static
75 and the dynamic coseismic displacements obtained from Very High-Rate GPS (VHRGPS)
76 measurements using a single station analysis approach. Previous work about VHRGPS data deals
77 with noise characteristics [*Genrich and Bock*, 2006] or on structural monitoring [*Ge et al.*, 2000;
78 *Çelebi and Sanli*, 2002; *Kogan et al.*, 2009], and VHRGPS solutions therein were obtained through
79 baselines estimates using a reference station. Our study, on the other hand, provides an
80 unprecedented opportunity to investigate near source dynamic displacements with VHRGPS, along
81 with near source frequency contributions of such a moderate magnitude earthquake. The L'Aquila
82 earthquake provided a large number of seismograms (http://iside.rm.ingv.it) and, as expected, the
83 short-period and broad-band seismometers available within ~10 km were clipped. However, the
84 mainshock was recorded by a number of strong motion (SM) stations (namely AQK, AQG, GSA
85 and GSG), belonging to the RAN (Rete Accelerometrica Nazionale) network of DPC
86 (http://www.protezionecivile.it/), and one accelerometer (AQU) of MedNet (INGV,
87 http://mednet.rm.ingv.it/). We will describe the analysis performed to retrieve the SM displacement
88 time series, and we will compare these results along with their spectral characteristics, with those
89 retrieved by the VHRGPS solutions of the closest sites. *Cirella et al.* [2009] used data of about 15
90 SM waveforms and 17 GPS static offsets within 70 km from the epicenter to image the rupture
91 history of this earthquake. Starting from this model, we will finally discuss the consistency of the

VHRGPS dynamic estimates with this previously determined model and the consistency of these VHRGPS results in relation to the selected seismic waveforms dataset.

2. 10 Hz GPS data analysis and results

2.1 VHRGPS data processing

[4] To analyze GPS data accurate satellite orbits and troposphere models are needed. Despite their own differences and peculiarities, scientific processing software packages [GAMIT, *Herring et al.*, 2006, BERNESE, *Beutler et al.*, 2007, and GIPSY/OASIS II, *Lichten and Borders*, 1987] use, for a given GPS network, double-differenced observations to resolve integer number phase ambiguity parameters. This approach provides more precise baseline daily repeatability compared to bias-free solutions. However, in the case of GIPSY/OASIS II software, the network solution step is preceded by the Precise Point Positioning (PPP) strategy, where receiver-specific parameters are estimated with receiver-specific data, fixing satellite-specific parameters [*Zumberge et al.*, 1997]. For our study, code and phase GPS data of the 10Hz sampling sites (ROIO and CADO) and of the two near field 1-Hz-sampling sites (INGP and INFN), were reduced by using the Gipsy-Oasis II (v.5.0) software PPP strategy in a kinematic mode (module *gd2p.pl*), as no 10-Hz-sampling GPS sites were operating in the far-field. We used JPL final high-rate (30s-sampled) fiducial orbits and high-rate (30s-sampled) clocks. The satellite orbits and clocks were held fixed to estimate receiver clocks, random walk zenith troposphere delay (by using values for slowly moving objects, i.e. ~3 mm/hr) [*Bar-Sever et al.*, 1998] and 10-Hz white noise (with 1 m *a-priori* standard deviation) receiver positions.

2.2 VHRGPS time series

114 [5] We compared the 10-Hz-sampled results to the 1-Hz-sampled ones (fig. 2). In ROIO, the
115 deformation starts 2.3 s after the nucleation, earlier than CADO, whose deformation starts later (3.7
116 s). This is because ROIO is closer to the earthquake nucleation point than CADO. For both sites,
117 the vertical components clearly show a subsidence occurred in three steps, reaching values
118 temporarily larger than the final co-seismic displacement. ROIO and CADO reached maximum
119 subsidence values of 13.9 cm and 17.7 cm, respectively. On the other hand, the horizontal
120 components show different behaviours. The first seismic pulses of ROIO are both positive on North
121 and East components, whereas CADO shows a mainly north-north-westward first horizontal pulse.
122 Furthermore, on the horizontal components, about 5 s after the beginning of the dynamic
123 deformation, both the 10-Hz GPS sites show a movement apparently regular in frequency (around 1
124 Hz) which starts with a high amplitude pulse, followed by a displacement that rapidly decreases in
125 amplitude and reaches the noise level after 6.5-6.8 s. The ROIO North and East displacements are
126 clearly *out-of-phase* (reaching maximum amplitude of 8.5 cm peak-to-peak), thus demonstrating
127 that this movement is mainly in the NW-SE direction (as the fault strike, fig. 1, and static
128 displacements direction). On the other hand, CADO shows a very high amplitude East and North
129 *in-phase* initial movement (up to 40cm peak-to-peak in the East component), that mainly occurs in
130 the NE-SW direction, fairly normal to the fault strike and in the direction of the coseismic static
131 displacements. This is not surprising because the initial P wave displacements can be very different
132 than the final coseismic displacements [*Vigny et al.*, 2010]. However, these high-amplitude
133 displacements are not observed at the closer SM stations [*Cirella et al.*, 2009].

134 [6] As highlighted by the ROIO and CADO 1-Hz solutions, the two 1-Hz sites INGP and INFN
135 cannot provide further details in the coseismic dynamic signals (fig. 2). INGP and INFN show
136 vertical offsets that are closer to or inside the noise level and they experienced lower co-seismic
137 displacements than ROIO and CADO (fig. 2). This could be related to the location of INGP and

INFN with respect to the fault: INGP is located on the NW unslipped border of the fault [*Cirella et al.*, 2009; *Cheloni et al.*, 2010] and *Pino et al.* [2009] showed that rupture propagated firstly up-dip and then mainly in the SE direction. Among the four GPS sites used in this study, INFN is the only one located on the footwall of the fault, relatively distant from the epicenter (about 14 km, ~1 rupture length).

[7] Previous studies [*Larson et al.*, 2001] indicated that the random walk noise should be used for position estimation in cases of slow deformation, such as volcanic or post-seismic deformation, for time windows that range from hours to days; in contrast, white noise should be used to estimate co-seismic (faster) dynamic deformation. We tested both white noise (with 1 m *a-priori* standard deviation) and random walk noise (with 1 m *a-priori* standard deviation and ~1.6 cm steady state standard deviation, Table SM1) for position estimation: in the 30 s time window spanning the earthquake, the results appear to be almost coincident (Fig. SM1). This is probably due to the very short time window covering the earthquake and to the relatively high signal to noise ratio (SNR). For the same reason (high SNR in a short time window), the contribution of the common-mode filtering [*Wdowinski et al.,* 1997] is considered negligible. To investigate if multipath can affect the GPS signals in short time windows, we determined the contribution of the sidereal filtering following the method described by *Choi et al.* [2004]. In the 30 s time window spanning the earthquake, for both the 10-Hz GPS sites, the differences between filtered and unfiltered signals show a low frequency trend (fig. SM2) and are well within the RMS of the VHRGPS time series (1.3, 0.6 and 3 cm for north, east and vertical components, respectively). Thus, we infer that, in this case, sidereal filtering does not significantly affect the high frequency coseismic dynamic displacements and it has not been applied.

[8] We have compared static displacements from VHRGPS to those obtained by daily averaging [*Anzidei et al.*, 2009, and *Cheloni et al.*, 2010] (fig. 2). Using position time series starting from

01:32:35 UTC, we calculated mean co-seismic offsets by differencing average positions in the 0-5 s and 25-30 s time windows (Table 1). We did not take into account the 5-25 s time window to avoid sampling co-seismic dynamic signal and we considered the 25-30 s time window assuming that no significant initial post-seismic deformation occurred. The differences between the offsets of the previously mentioned studies and the kinematic solutions of our study (with or without sidereal filtering) are outside the error uncertainties for each site. These differences can be mainly due to the fact that the April 6th daily estimations, propagated at 12:00 UTC, could be affected by an early aseismic post-seismic deformation, as suggested also by *D'Anastasio et al.* [2009]. In this sense, for the L'Aquila earthquake, as for the Parkfield earthquake [*Johnson et al.*, 2006], the measurements of the co-seismic static displacements provided by the VHRGPS solutions are more accurate than those derived by the daily solutions.

2.3 VHRGPS three-component spectra

[9] To investigate the frequency contributions present in the HRGPS (10 Hz and 1 Hz) signals, we estimated Power Spectral Density (PSD). For this purpose, we used a GMT package tool (*spectrum1d*, http://gmt.soest.hawaii.edu/) based on the Welch's method of ensemble averaging of multiple overlapped windows, considering standard error estimates [*Press et al.*, 1992]. We calculated PSDs of the instantaneous sites positions in a 20 min time window including the mainshock ("coseismic PSD"). For ROIO and CADO, the PSD was calculated both for the 10-Hz solution and the 1-Hz decimated solution, whereas for INFN and INGP, the PSD was calculated for the only available 1-Hz solution (fig. 3). The horizontal components of ROIO and CADO are characterized by an apparent PSD peak in the 0.7-1 Hz frequency range. This corresponds to the high-amplitude signal visible in the time series (fig. 2a,b). In the 1-Hz PSD (with Nyquist frequency at 0.5 Hz), this frequency contribution peak is reflected off at frequencies ~0.09-0.3 Hz. This feature points out aliasing in the 1-Hz GPS signal, in agreement with previous hypothesis [*Smalley*,

186 2009]. Furthermore, the PSDs of the 10-Hz solutions follow the expected spectral decay of the
187 source radiated displacement spectrum [*Aki*, 1967; *Brune*, 1970, 1971] up to ~2 Hz. Above this
188 frequency, the PSDs appear to be flat. To investigate the levels of noise at ROIO and CADO, we
189 calculated PSDs of the 10-Hz solution for the three components in a 20 min time window before the
190 earthquake occurrence ("preseismic PSD") (fig. 3). As shown for the 1-Hz PSDs of ROIO and
191 CADO, also the coseismic PSDs of the 1-Hz solutions of INGP and INFN point out a relatively
192 significant aliasing contribution. For the 10-Hz solutions, below ~2 Hz, the preseismic PSDs of the
193 horizontal components show energy levels (Table 2) that on average are significantly lower than the
194 coseismic PSDs. On the other hand, above 2 Hz, the preseismic and the coseismic PSDs overlap,
195 reaching noise levels of ~0.7 mm and ~0.9 mm for the east and north components, respectively. For
196 the vertical components, the preseismic and coseismic PSD differences appear more complicated up
197 to ~1 Hz: at CADO, the coseismic PSDs show peaks until they overlap the preseismic PSD (above
198 ~1 Hz). On the other hand, ROIO shows a smaller energy difference, gradually decreasing, until the
199 two signals have almost reached the same levels (above ~0.8 Hz). Above 0.8-1 Hz, both sites
200 vertical components reach noise levels of ~1.4 mm. We summarize as follows: first, the differences
201 in the energy levels appear in the frequency range of the coseismic displacements (both static and
202 dynamic), thus indicating that the observed coseismic dynamic signal is largely above the noise
203 level; second, the overlapping of the preseismic and coseismic PSDs at higher frequencies (~2 Hz
204 for the horizontal components and ~1 Hz for the vertical one) suggests that the noise level is
205 reached.

206 [10] We investigated the noise level of PPP kinematic solutions at higher frequencies, performing a
207 1-hr spanning 20-Hz sampling test on a RING network CGPS site (GRO1) (fig. 4). This CGPS site
208 is equipped with the same instrumentation engine (Leica GRX1200) as the receivers at ROIO and
209 CADO (Leica GRX1230), but with a different antenna (Leica AT504, Dorne Margolin with

chokerings). The PSD functions of the 20-Hz solutions become flat above 1 Hz but they reach energy values that are ~2-3 times lower than the PSDs of the GRO1 10-Hz solutions (Table 2). However, it remains to understand if the energy levels observed at high frequencies for the 10-Hz and 20-Hz solutions are representative of the VHRGPS noise level or they are affected by aliasing. The best way to answer this question is to compare the VHRGPS signal with independent data that have sampling rates normally higher than GPS, such as the "quasi-co-located" SM data.

3. **Strong motion data analysis and Comparison with VHRGPS data**

3.1 Strong motion data analysis

[11] Among the SM stations that were triggered by the April 6th L'Aquila mainshock, we selected only near-field SM sites (AQU, AQK, AQG, GSA and GSG). These sites are close enough to the GPS sites to be considered "quasi-collocated" in relation to the seismic waves wavelength (~2-5 km). Thus, a comparison between the two datasets can be performed. In order to obtain displacement time series from accelerograms, a double integration has been performed in the time domain. Double integration is known to involve distortion and residual trends in the final displacement time histories. Conventional procedures based on high-pass filtering fail in yielding acceptable results, because they remove the desired signal. As suggested by *Boore and Bommer* [2005], a baseline correction in the time domain has to be used. We therefore adopted a procedure recently modified by C. Di Alessandro and G. Calderoni (INGV) from the Paolucci's BASCO (BASeline COrrection) code [*Faccioli and Rovelli*, 2007]. In the original code, acceleration is integrated and the resulting velocity time history is segmented in several portions, in each of them the linear trend is removed in a trial-and-error approach. The implemented software searches for the number and length of the segments through an automatic grid-search, the best solution being the

233 one which retrieves the most stable trend in the static displacement. For small magnitude
234 earthquakes and long distances, the code converges towards the solution associated with a minimum
235 residual offset in the last portion of the displacement time series. When a permanent displacement is
236 expected, i.e. for moderate to large magnitude at near source distance, the solution is selected so
237 that it provides the most stable constant offset in the final asymptotic part of the displacement time
238 series for at least 10-20 seconds, after the completed dislocation of the fault. The coseismic offsets
239 observed at SM stations are summarized in Table 1.

240 *3.2 Comparison between VHRGPS and strong motion: time series*

241 [12] Previous studies [*Larson et al.*, 2003; *Miyazaki et al.*, 2004, *Emore et al.*, 2007; *Yokota et al.*,
242 2009] showed that GPS can detect seismic waves (mainly surface waves) for large earthquakes,
243 comparing 1-Hz-sampled GPS position time series with SM data. In the case of the L'Aquila
244 earthquake, we have the first 10-Hz-GPS dataset collected in the near-field of a relatively large
245 earthquake. A reliable detection of coseismic displacements from SM over tens of seconds [*Boore*,
246 2001; *Wang et al.*, 2007], despite potentially important rotational components of the shaking
247 [*Trifunac*, 1982; *Graizer*, 1989; *Graizer*, 2006], is still a matter of debate. As most of the sites are
248 not exactly in the same place, the beginning of the deformation occurs at slightly different times due
249 to differences in the seismic wave propagation time. Thus, the comparison VHRGPS-SM cannot be
250 properly useful to assess the reliability of the SM static offset. On the other hand, it is interesting to
251 highlight the agreement within ±1 cm accuracy of the position time series between those closely-
252 spaced sites showing similar features for the vertical component (between CADO and AQU/AQK,
253 Fig. 5a) and for the horizontal components (between ROIO and AQU/AQK, Fig. 5b). Also INGP (1
254 Hz) show features on the east and vertical components that are similar (within ± 1 cm) to the closest
255 SM site AQG (Fig. 5c), but, as INGP is located near the source, the 1-Hz GPS signal is affected by
256 aliasing. To properly investigate the reliability of the retrieved SM coseismic offset, we limit the

comparison to the only case of co-located VHRGPS-SM stations. The 1-Hz GPS INFN is co-located with GSA and close (~5 km) to GSG. The results show a good agreement (fig. 5c). The horizontal components have the same peaks of the INFN time series even with some differences in amplitude: for the north component, INFN appears similar to GSA, whereas for the east component, INFN time series is similar to GSG. The lower signal amplitude on the vertical component for GSG can be explained by its location in a borehole. On the north component, INFN seems to diverge significantly from the SM solutions. However, we show that the SM displacements seem to be quite stable over a period of about 40 s after the earthquake.

3.2 Comparison between VHRGPS and strong motion: three-component spectra

[13] The GPS-SM comparison is also performed by means of three-component spectra (fig.5d, Table 3) in the time window used for calculating displacements from SM (45 s). We will only focus on the PSD comparison between the 10-Hz GPS sites (ROIO and CADO) and the two closest SM sites (AQU and AQK). To better compare the two datasets we impose an upper boundary to the PSD plots at 6 Hz, a little more than the Nyquist frequency of the 10-Hz GPS signal (5 Hz). At low frequencies (below 0.3 Hz), the PSDs appear comparable for all the components. The variability for the East and North components are confined to the 1-8 cm^2/Hz and the 10-20 cm^2/Hz energy ranges, respectively. At AQK, we observe a wide peak at ~0.5-0.6 Hz on the horizontal components and the 1-Hz peak on the vertical component. At slightly higher frequencies (0.7-1 Hz), CADO shows larger energy than the other PSDs, reaching maximum PSD values of ~6 and ~21 cm^2/Hz for the north and east components, respectively (fig.5d, Table 3). ROIO reaches energy values comparable to CADO at ~1 Hz, but still larger than the SM data. However, with the exception of the above described peaks, all the PSD functions show the same decay of energy with increasing frequency. Above 2 Hz, not only the 10-Hz GPS PSDs significantly diverge from the SM PSDs, but also the GPS PSDs themselves appear different: on the vertical component, both CADO and ROIO

clearly overlap and become almost flat at an average energy level of ~1*10^{-2} cm^2/Hz; on the horizontal components, CADO shows a sawtooth-like aspect with one order of magnitude energy variations; in ROIO it is possible to see a similar behaviour but with lower energy variations. However, the lower PSDs levels are reached in the range 10^{-3}-10^{-2} cm^2/Hz (fig.5d). For the three components, the SM PSDs decay until 5 Hz reaching energy values of two orders of magnitude lower than GPS (~10^{-4} and ~10^{-5} cm^2/Hz for AQK and AQU, respectively). These PSDs values at high frequencies in the SM data suggest that aliasing contribution, if it exists, is very low and the comparison between VHRGPS and SM PSDs confirms that no aliasing contribution affects the 10-Hz GPS signal.

4. Kinematic rupture history

[14] In order to assess the consistency of the VHRGPS coseismic dynamic displacements, we modelled the kinematic rupture history of the 2009 L'Aquila main-shock. For this purpose, we jointly inverted strong ground motions records, dynamic and static GPS displacements by using a two-stage nonlinear inversion method [*Piatanesi et al.*, 2007]. We assumed the same fault geometry (28 km long and 17.5 km wide, strike fault: N133°E; dip to SW: 54°; top of the fault: 0.5 km) and approximately the same site selection described by *Cirella et al.* [2009]. Particularly, in our study we considered the AQK accelerograms (RAN network) along with the dynamic and static displacements obtained from the VHRGPS kinematic analysis related to four GPS sites (ROIO, CADO, INFN, INGP, fig. 6). With the exception of these four GPS sites, all the other GPS offsets are the same as those used in *Cirella et al.* [2009] and derived by previous daily static analysis [*Anzidei et al.*, 2009]. Original acceleration recordings and high-rate dynamic GPS are integrated and derived, respectively, to obtain ground velocity time histories. The resulting velocity waveforms are band-pass filtered between 0.02 and 0.5 Hz by using a two-pole and two-pass

305 Butterworth filter. We inverted 60 s of each waveform; this includes body and surface waves. All
306 kinematic parameters are simultaneously inverted at nodal points every 3.5 km equally spaced along
307 strike and dip directions. During the inversion, the peak slip velocity is allowed to vary between 0
308 and 2.5 m/s with 0.25 m/s step increment and the rise time between 1 and 2 s with 0.25 step
309 increment. The rake angle ranges between 250° and 290° with 5° step increments; the rupture time
310 distribution is constrained by a rupture velocity ranging between 1.8 and 2.8 km/s. To calculate the
311 Green's functions, we adopted a velocity model retrieved from receiver functions [*Bianchi et al.*,
312 2010] to compute the synthetic seismograms at AQU, AQG and AQK. For all the other stations we
313 use a model based on the 1-D structure of *Bagh et al.* [2007] modified to take into account the
314 shallow (0-1.5 km) low velocity layer. The body-wave velocities in this shallow layer are taken
315 from a 1-D structure (nnCIA model) obtained from surface wave dispersion analysis [*Hermann and*
316 *Malagnini*, 2009].

317 [15] The algorithm explores ~2 millions rupture models to build up the model ensemble. Figure 6
318 shows the retrieved slip distribution, either on the fault plane or projected on the Earth surface,
319 obtained by averaging a subset of the model ensemble (nearly 30.000 rupture models),
320 corresponding to those models having a cost function not exceeding 5% of the minimum cost
321 function value (i.e., the best fitting model). The retrieved model presents similar features compared
322 to *Cirella et al.* [2009] (fig. SM3) and it is characterized by three principal patches of slip: the
323 largest patch is near the nucleation point, 8 km SE from the nucleation, a second smaller slip patch
324 above the hypocenter at shallower depths (i.e., nearly 3 km in the up-dip direction) and a third, 3 km
325 NW below the hypocenter. The larger asperity reaches a maximum slip of about 1.1 m, whereas the
326 shallower and the northwestern patches reach maximum slips of nearly 0.7 m and 0.8 m,
327 respectively. The rake angle in correspondence of the maximum slip is -102° and the resulting
328 seismic moment ($M_0 = 3.5 \times 10^{18}$ Nm) agrees fairly well with Regional Centroid Moment Tensor

329 solution. It's important to remark that several seismic and GPS stations lie on the hanging wall of
330 the causative fault as displayed in figure 6 where we already showed the match between the
331 observed and synthetic GPS static offsets (red and blue vectors, respectively). Our kinematic
332 rupture model, that includes the dynamic and static VHRGPS displacements, is comparable to the
333 one proposed by *Cirella et al.* [2009] (fig. SM3). This is not surprising considering that VHRGPS
334 data represent a minority (4) compared to the total number of waveforms (19) used for the
335 inversion. This result shows the consistency of the kinematic VHRGPS time series with the other
336 seismological and geodetic dataset collected during the 2009 L'Aquila earthquake (fig. 7). In fact,
337 the synthetic ground velocities match fairly well the recorded seismograms at most of the stations
338 (fig. 7a). Discrepancies at some sites are probably due to the inadequate modelling of the complex
339 wave propagation (high-amplitude signal at ROIO and CADO) and the inadequate accounting of
340 the site effects (AQK) (both not included in our simulations). Also the fit (fig. 7b) of the four high-
341 rate dynamic GPS displacements is satisfactory, with the exception of INGP, which could be
342 affected by aliasing. Although, the 1-Hz high-amplitude signal is not modelled because our model
343 spans the 0.02-0.5 Hz range, the beginning of the signal of the horizontal components and the signal
344 of the vertical component is well reproduced.

345

346 **Discussion**

347 [16] The PSD functions at AQK (fig.5d) show peaks at 0.5-0.6 Hz that have been previously
348 observed during other earthquakes [*De Luca et al.*, 2005] as well as during the L'Aquila earthquake
349 [*Akinci et al.*, 2010]. These peaks have been interpreted as a site effect due to ~400 m deep
350 L'Aquila basin composed of alluvial deposits of the Aterno valley [*Agency for Environmental*
351 *Protection and Technical Services (APAT), 2005*]. The PSD functions of the horizontal components
352 at the GPS sites closer to AQK (ROIO and CADO) show peaks at slightly higher frequencies (~1

353 Hz and 0.7-1 Hz, respectively). However, both the GPS stations are installed on limestone outcrops,
354 whereas AQK is located in the L'Aquila basin. The monumentation at ROIO and CADO is a
355 concrete pillar and the GPS antenna was screwed on the top of the pillar, which was further fixed by
356 using cement. Therefore, a site effect caused by a variation of shear velocity due to soft uppermost
357 layers has to be excluded. However, ground motions recorded at stations located on the top of
358 topographic irregularities could be affected by a local amplification (i.e. topographic effect), but this
359 effect should cause an amplification of the whole seismic signal, not a part of it [*Geli et al.*,1988;
360 *Bouchon and Barker*, 1996; *Paolucci*, 2002]. In the case of ROIO and CADO, the high-amplitude
361 signals do not affect the first seismic arrivals, which are, conversely, well-fit by the kinematic
362 rupture model (fig.7a,b); the large amplitude portion of GPS signals occurs about 5 s after the
363 beginning of the deformation and spans about 6.5-6.8 s. Furthermore, the high-amplitude signal
364 cannot be related to a source effect (i.e. stopping phase) because of its low-frequency nearly-
365 harmonic signature. *Avallone et al.* [2010a] attempted to model this feature as a fault zone
366 resonance (*Ben-Zion and Aki*, 1990; *Li and Leary*, 1990), the two GPS receivers being located on
367 fault systems close to the causative Paganica fault.
368 [17] The GPS-SM comparison, as well as the comparison between the preseismic and the coseismic
369 PSDs, suggests that the minimum energy levels of the 10-Hz GPS data can be representative of the
370 noise levels of the VHRGPS data, because the aliasing contributions reach energy levels that are
371 two orders of magnitude lower than the GPS signal at high frequencies (4.5-5 Hz). This also
372 suggests two aspects: first, a higher sampling (i.e. 20 Hz) would not have provided additional
373 information, in terms of frequency, for the L'Aquila earthquake; second, aliasing on near-source
374 high-rate GPS data can occur only by sampling data at frequencies lower or equal to 5 Hz (Nyquist
375 frequency $\leq$ 2.5 Hz), as confirmed by the previously described 1-Hz solutions of CADO and ROIO
376 (fig. 3) and suggested by previous studies on strong motion data [*Smalley*, 2009]. This is probably
377 the case of the 1-Hz-sampling INGP receiver. In fact, the projection on the Earth surface of the

kinematic rupture model obtained using the VHRGPS data (fig. 6a) shows the presence of a significant patch of slip below INGP, deeper than the nucleation point and amounting up to 0.8 m of slip. This patch represents the main difference between the rupture model obtained in our study compared to the one of *Cirella et al.* [2009] and the fit of both the static (fig. 6) and the dynamic (fig. 7) INGP displacements are relatively low. On the contrary, for the three other GPS sites (ROIO, CADO and INFN), the fit of the waveforms appears satisfactory and the fit of the static displacements is better (fig.6) than the one found in *Cirella et al.* [2009]. This suggests that the other 1-Hz GPS site (INFN) may not be affected by aliasing due to attenuation of the high frequency components on the longer travel path. This result suggests that a 1-Hz-sampling GPS site located in the near source of a moderate magnitude event (M 6 class) provides an aliased solution, that can significantly affect the resulting kinematic rupture model.

Conclusions

[18] The VHRGPS data acquired during the 2009 Mw 6.3 L'Aquila earthquake are the first time that 10-Hz GPS data have been recorded in the near-field of the fault rupture. *Yokota et al.* [2009] demonstrated that 1-Hz GPS data alone, located in the far-field, are able to infer the dynamic features of the rupture process as well as permanent slip even for a Mw 6.9 earthquake. Our study showed that opportunely-located and very high-rate-sampling GPS sites are able to detect also the first seismic arrivals of moderate magnitude earthquakes (Mw 6.3). Thus, as suggested by *Genrich and Bock* [2006], dense VHRGPS networks will be very helpful to detect significant variations in the seismic wave propagation, that could be related to rupture dynamics or otherwise hidden geologic heterogeneities. In Italy, a significant effort has been made to develop a high-quality real-time-telemetered dense CGPS network, where the CGPS sites are, in most cases, co-located with broad-band and strong motion instruments [RING network, http://ring.gm.ingv.it, *Avallone et al.*,

402 2010b]. A further effort to increase the density of high-rate sampling CGPS sites in the seismogenic
403 structures areas (i.e. every 5-10 km or with inter-distances < 1 length of a typical moderate
404 magnitude fault size) could potentially provide an important complementary network to explore the
405 full range of temporal and spatial frequencies that characterize plate boundary deformation, from
406 regional plate kinematics to earthquake source studies.

407 [19] Our study confirms that recording frequencies greater than 2.5 Hz are needed for detailed
408 studies on rupture process of moderate magnitude events through GPS dynamic displacements.
409 Observations at high frequencies (>2.5 Hz) indicate that the aliasing contribution is too low to be
410 observed. Furthermore, the 20-Hz solutions [*our study* and *Genirch and Bock*, 2006] or the 50-Hz
411 solution [*Genrich and Bock*, 2006] (Table 2) show energy levels at Nyquist frequencies two-three
412 times lower than the 10-Hz solutions, but still three-four times larger than the observed aliasing
413 contribution in the SM displacements (fig. 5d). Higher sampling rates (20 Hz or more) may be
414 useful for other earthquakes and a proper filtering and averaging of these data would allow more
415 precise VHRGPS position estimates at lower frequencies (10 Hz). However, higher sampling rates
416 would not have provided additional information for the L'Aquila earthquake. Moreover, sampling
417 GPS data at 10 Hz could represent a good trade-off between 1 Hz and 20 Hz (or higher), allowing to
418 locally store a reasonable amount of data (~330Mb/day) in a frequency range useful for
419 seismological studies.

420 [20] 10-Hz GPS results have been obtained using a single station (PPP) kinematic approach. This
421 approach turned out to be crucial for the L'Aquila earthquake as no 10-Hz GPS were operating in
422 central Italy. The kinematic approach represents a powerful strategy to analyze relatively short data
423 time windows (i.e. 30 s), such as data related to moderate magnitude events in the near field. We
424 demonstrated that the single-point (without bias-fixing) kinematic results provide precisions
425 comparable to baseline solutions [*Genrich and Bock*, 2006]. A next step forward, as the possibility

426 to routinely include ambiguity phase resolution for single station data analysis [*Bertiger et al.*,
427 2010], would make the PPP strategy more accurate. It could be useful to detect displacements of
428 lower magnitude, or deeper, earthquakes and its results could be comparable to baseline solutions.

429

430 **Acknowledgements**

431 We are grateful to Roberto Devoti, Marco Anzidei, Angelo Massucci and Sergio Del Mese, who
432 installed and maintained the 10 Hz-sampling GPS stations at CADO and ROIO before, during and
433 after the L'Aquila earthquake. We thank the staffs of the Istituto Nazionale di Geofisica e
434 Vulcanologia (INGV) and the Dipartimento Protezione Civile (DPC) for the development and
435 maintenance of the RING and RAN networks, respectively. Uncorrected mainshock strong motion
436 recordings have been obtained from the ITalian ACcelerometric Archive (ITACA,
437 http://itaca.mi.ingv.it). The first author thanks André Herrero and Aladino Govoni for helpful
438 discussions about signal spectral analysis. We also thank Robert Nowack, the Associated Editor,
439 Kristine M. Larson and an anonymous reviewer for constructive observations, which helped to
440 increase the quality of the manuscript. This research has benefited from funding provided by the
441 Italian Presidenza del Consiglio dei Ministri-Dipartimento della Protezione Civile (DPC-S5-
442 WP3.4). Scientific papers funded by DPC do not represent its official opinion and policies. M.M. is
443 supported by the same project. Figures have been prepared using GMT software package [*Wessel*
444 *and Smith*, 1998].

445

446 **References**

447 Agency for Environmental Protection and Technical Services (APAT) (2005), Carta Geologica
448 d'Italia, F.° 359 L'Aquila, scale 1:50,000, APAT (Servizio Geologico d'Italia) and Regione
449 Abruzzo, S.EL.CA, Firenze.

450 Aki, K. (1967). Scaling law of seismic spectrum, *J. Geophys. Res.*, 72, 1217-1231.

451 Akinci, A., L. Malagnini and F. Sabetta (2010), Characteristics of the strong ground motions
452 from the 6 April 2009 L'Aquila earthquake, Italy, *Soil Dynamics and Earthquake Engineering*, 30,
453 320-335, doi:10.1016/j.soildyn.2009.12.006.

454 Anzidei, M., E. Boschi, V. Cannelli, R. Devoti, A. Esposito, A. Galvani, D. Melini, G.
455 Pietrantonio, F. Riguzzi, V. Sepe and E. Serpelloni (2009), Coseismic deformation of the
456 destructive Aprile 6, 2009 L'Aquila earthquake (central Italy) from GPS data, *Geophys. Res. Lett.*,
457 36, L17307, doi:10.1029/2009GL039145.

458 Argus, D. F., and M. Heflin (1995), Plate motion and crustal deformation estimated with
459 geodetic data from the Global Positioning System, *Geophys. Res. Lett.*, 22, 1973–1976.

460 Avallone, A., A. Rovelli, Y. Ben-Zion (2010a), Trapped seismic fault zone energy recorded by a
461 high-rate GPS station, *Eos Trans. AGU*, Fall Meet. Suppl., Abstract T53C-2142, December 2010.

462 Avallone A., G. Selvaggi, E. D'Anastasio, N. D'Agostino, G. Pietrantonio, F. Riguzzi, E.
463 Serpelloni, M. Anzidei, G. Casula, G. Cecere, C. D'Ambrosio, P. De Martino, R. Devoti, L. Falco,
464 M. Mattia, M. Rossi, F. Obrizzo, U. Tammaro and L. Zarrilli (2010b), The RING network: an
465 improvement of the GPS velocity field in the Central Mediterranean area, *Annals of Geophysics*, 51
466 (2).

467 Bagh, S., L. Chiaraluce, P. De Gori, M. Moretti, A. Govoni, C. Chiarabba, P. Di Bartolomeo and
468 M. Romanelli (2007), Background seismicity in the Central Apennines of Italy: The Abruzzo region
469 case study, *Tectonophysics*, 444, 80-92, doi:10.1016/j.tecto.2007.08.009.

470 Bar-Sever, Y. E., P. M. Kroger, and J. A. Borjesson (1998), Estimating horizontal gradients of
471 tropospheric path delay with a single GPS receiver, *J. Geophys. Res.*, 103(B3), 5019–5035.

472 Ben-Zion, Y., and K. Aki (1990). Seismic radiation from an SH line source in a laterally
473 heterogeneous planar fault zone, *Bull. Seism. Soc. Am.,* 80**,** 971–994.

474 Bertiger, W., S. Desai, B. Haines, N. Harvey, A. Moore, S. Owen, J. Weiss (2010), Single
475 receiver phase ambiguity resolution with GPS data, *Journal of Geodesy*, 84, 5 (May 2010), pp. 327-
476 337.

477 Beutler, G., et al. (2007), Bernese GPS Software. In: Dach R., Hugentobler U., Fridez P.,Meindl
478 M. (Eds), Astronomical Institute, University of Bern (January 2007).

479 Bianchi, I., C. Chiarabba and N. Piana Agostinetti (2010), Control of the 2009 L'Aquila
480 earthquake, central Italy, by a high velocity structure: a Receiver Function study, *submitted to J.*
481 *Geophys. Res.*

482 Blewitt, G. (1989) Carrier phase ambiguity resolution for the global positioning system applied
483 to geodetic baselines up to 2,000 km, *J. Geophys. Res.*, 94(B8),10187-10203,
484 doi:10.1029/89JB00484.

485 Blewitt, G., C. Kreemer, W. C. Hammond, H.-P. Plag, S. Stein, and E. Okal (2006), Rapid
486 determination of earthquake magnitude using GPS for tsunami warning systems, *Geophys. Res.*
487 *Lett.,* Vol. 33, L11309, doi:10.1029/2006GL026145.

Blewitt, G. (2008), Fixed point theorems of GPS carrier phase ambiguity resolution and their application to massive network processing: Ambizap, *J. Geophys. Res.*, 113, B12410, doi:10.1029/2008JB005736.

Bock, Y., R. M. Nikolaidis, P. J. De Jonge, and M. Bevis (2000), Instantaneous geodetic positioning at medium distances with Global Positioning System, *J. Geophys. Res.*, 105(B12), 28,223-28,253, doi:10.1029/2000JB900268.

Bock, Y., L. Prawirodirdjo, and T. I. Melbourne (2004), Detection of arbitrarily large dynamic ground motions with a dense high-rate GPS network, *Geophys. Res. Lett.*, 31, L06604, doi:10.1029/2003GL019150.

Boncio, P., G. Lavecchia, G. and B. Pace (2004) Defining a model of 3D seismogenic sources for Seismic Hazard Assessment applications: the case of central Apennines (Italy), *J. Seismol.,* 8**,** 407–425.

Boore, D. M. (2001). Effect of baseline correction on displacement and response spectra for several recordings of the 1999 Chi-Chi, Taiwan, earthquake, *Bull. Seism. Soc. Am.*, 91**,** 1199–1211.

Boore, D. M. and J. J. Bommer (2005), Processing of strong-motion accelerograms: needs, options and consequences, *Soil Dynamics and Earthquake Engineering*, 25, 93-115.

Bouchon, M. and J.S. Barker (1996), Seismic response of a hill: The example of Tarzana, California, *Bull. Seism. Soc. Am.*, 86, 66-72.

Brune, J. N. (1970), Tectonic stress and spectra of seismic shear waves from earthquakes, *J. Geophys. Res.*, 75, 4997-5009.

Brune, J. N. (1971), Correction, *J. Geophys. Res.*, **76,** 5002.

509 Çelebi, M. and A. Sanli (2002), GPS in pioneering dynamic monitoring of long-period
510 structures, *Earthquake Spectra*, 18, 47-61.

511 Cheloni, D., N. D'Agostino, E. D'Anastasio, A. Avallone, S. Mantenuto, R. Giuliani, M.
512 Mattone, S. Calcaterra, P. Gambino, D. Dominici, F. Radicioni and G. Fastellini (2010), Coseismic
513 and initial postseimic slip of the 2009 Mw 6.3 L'Aquila earthquake, Italy, from GPS measurements,
514 *Geophys. J. Int.*, 181, 1539-1546, doi: 10.1111/j.1365-246X.2010.04584.x.

515 Chiarabba, C., et al. (2009), The 2009 L'Aquila (central Italy) MW6.3 earthquake: Main shock
516 and aftershocks, Geophys. Res. Lett., 36, L18308, doi:10.1029/2009GL039627.

517 Choi, K., A. Bilich, K. M. Larson, and P. Axelrad, Modified sidereal filtering: Implications for
518 high-rate GPS positioning Geophys. Res. Lett., Vol. 31, No.22, L22608, doi
519 10.1029/2004GL021621, 2004

520 Cirella, A., A. Piatanesi, M. Cocco, E. Tinti, L. Scognamiglio, A. Michelini, A. Lomax and E.
521 Boschi (2009), Rupture history of the 2009 L'Aquila (Italy) earthquake from non-linear joint
522 inversion of strong motion and GPS data, *Geophys. Res. Lett.*, 36, L19304,
523 doi:10.1029/2009GL039795.

524 D'Agostino, N., D. Cheloni, S. Mantenuto, G. Selvaggi, A. Michelini, and D. Zuliani (2005),
525 Strain accumulation in the southern Alps (NE Italy) and deformation at the northeastern boundary
526 of Adria observed by CGPS measurements, Geophys. Res. Lett., 32, L19306,
527 doi:10.1029/2005GL024266.

528 D'Anastasio, E., G. Blewitt, N. D'Agostino, A. Avallone, D. Cheloni and M. Marzario (2009),
529 The 2009 L'Aquila Earthquake: Postseismic Deformation with High Temporal Resolution Using the
530 new GPS "Carrier Range" Data Type, *Eos Trans. AGU*, 90(52), Fall Meet. Suppl., Abstract G31A-
531 05.

532 Davis, J. P. and R. Smalley Jr. (2009), Love wave dispersion in central North America
533 determined using absolute displacement seismograms from high-rate GPS, J. Geophys. Res., 114,
534 B11303, doi:10.1029/2009JB006288.

535 De Luca. G., S. Marcucci, G. Milana and T. Sanò (2005), Evidence of Low-Frequency
536 Amplification in the City of L'Aquila, Central Italy, through a Multidisciplinary Approach
537 Including Strong- and Weak-Motion Data, Ambient Noise, and Numerical Modeling, *Bull. Seism.*
538 *Soc. Am.*, 95, 4, 1469–1481, doi: 10.1785/0120030253.

539 Dixon, T. H. (1991), An introduction to the Global Positioning System and some geological
540 applications, *Rev. Geophys.*, 29, 249–276.

541 Dragert, H., K. Wang, and T. S. James (2001), A silent slip event on the deeper Cascadia
542 subduction interface, *Science*, 292, 1525-1528, doi:10.1126/science.1060152.

543 Emergeo Working Group, 2009. Evidence for surface rupture associated with the Mw 6.3
544 L'Aquila earthquake sequence of April 2009 (central Italy), *Terra Nova,* 22**,** 43–51,
545 doi:10.1111/j.1365-3121.2009.00915.x.

546 Emore, G., J. Haase, K. Choi, K. M. Larson, and A. Yamagiwa (2007), Recovering absolute
547 seismic displacements through combined use of 1-Hz GPS and strong motions accelerometers, *Bull.*
548 *Seismol. Soc. Am.*, 97(2), 357-378, doi: 10.1785/0120060153.

549 Faccioli, E. and A. Rovelli (2007), Definizione dell'input sismico sulla base degli spostamenti
550 attesi. Progetti sismologici di interesse per il DPC - Relazione scientifica finale
551 http://progettos5.stru.polimi.it/Rendiconti.html.

552 Falcucci, E. *et al.*, 2009. The Paganica fault and surface coseismic ruptures caused by the 6 April
553 2009 earthquake (L'Aquila, Central Italy), *Seism. Res. Lett.,* 80(6), doi:10.1785/gssrl.80.6.940.

554 Fialko, Y. (2006), Interseismic strain accumulation and the earthquake potential on the southern
555 San Andreas fault system, *Nature*, 441, 969-971, doi: 10.1038/nature04797.

556 Galli, P., F. Galadini and D. Pantosti (2008), Twenty years of paleoseismology in Italy, *Earth*
557 *Sci. Rev.,* 88(1–2), 89–117, doi:10.1016/j.earscirev.2008.01.001.

558 Ge, L., S. Han, C. Rizos, Y. Ishikawa, M. Hoshiba, Y. Yoshida, M. Izawa, N. Hashimoto, and S.
559 Himori (2000), GPS Seismometers with up to 20 Hz Sampling Rate, *Earth Planets Space*, 52(10),
560 881-884.

561 Geli L., P.-Y. Bard, B. Jullien (1988). The effect of topography on earthquakes ground motion: a
562 review and new results, *Bull. Seism. Soc. Am.*, 78, 42-63.

563 Genrich, J. F. and Y. Bock (2006), Instantaneous geodetic positioning with 10-50 Hz GPS
564 measurements: Noise characteristics and implications for monitoring networks, *J. Geophys. Res.*,
565 111, B03403, doi:10.1029/2005JB003617.

566 Graizer, V. M. (1989), Bearing on the problem of inertial seismometry. Izv USSR Acad Sci,
567 Physics Solid Earth **25**: 1, 26-29.

568 Graizer, V. M. (2006), Tilts in strong ground motion, *Bull. Seism. Soc. Am.*, 96, 6, 2090–2102,
569 doi: 10.1785/0120060065.

570 Hermann, R. B. and L. Malagnini (2009), Systematic determination of moment tensor of the
571 April 6th, 2009 L'Aquila earthquake sequence, *Eos Trans. AGU*, Fall Meet. Suppl., Abstract,
572 U23A-0029.

573 Herring, T. A., R. W. King and S. C. McClusky (2006) GPS Analysis at MIT, GAMIT
574 Reference Manual, Release 10.3. Department of Earth, Atmospheric, and Planetary Sciences

575 Massachusetts Institute of Technology, Cambridge MA
576 (http://chandler.mit.edu/~simon/gtgk/GAMIT_Ref_10.3.pdf).

577 Ji C., K. M. Larson, Y. Tan, K. W. Hudnut, K. Choi (2004), Slip history of the 2003 San Simeon
578 earthquake constrained by combining 1-Hz GPS, strong motion, and teleseismic data, *Geophys.*
579 *Res. Lett.*, 31, L17608, doi:10.1029/2004GL020448.

580 Johnson, K. M., R. Burgmann and K. Larson (2006), Frictional properties on the San Andreas
581 Fault near Parkfield, California, inferred from models of afterslip following the 2004 earthquake,
582 *Bull. Seism. Soc. Am.*, 96, 48, S321-S338, doi: 10.1785/0120050808.

583 Kogan, G. M., W.-Y. Kim, Y. Bock and A. W. Smyth (2008), Load Response on a Large
584 Suspension Bridge during the NYC Marathon Revealed by GPS and Accelerometers,
585 *Seism. Res. Lett.*, 79, 12-19.

586 Larson, K. M., J. T. Freymueller, and S. Philipsen (1997), Global plate velocities from the
587 Global Positioning System, *J. Geophys. Res.*, 102, 9961–9981.

588 Larson, K. M., P. Cervelli, M. Lisowski, A. Miklius, P. Segall, and S. Owen (2001), Volcano
589 monitoring using GPS: Filtering Strategies, *J. Geophys. Res.*, 106, 19453-19464,
590 doi:10.1029/2001JB000305.

591 Larson, K., P. Bodin, and J. Gomberg (2003), Using 1 Hz GPS Data to Measure Deformations
592 Caused by the Denali Fault Earthquake, *Science*, 300, 1421-1424.

593 Larson, K.M., V. Kostoglodov, A. Lowry, W. Hutton, O. Sanchez, K. Hudnut, and G. Suarez
594 (2004), Crustal Deformation Measurements in Guerrero, Mexico, *J. Geophys. Res.*, 109, B4,
595 B04409, doi:10.1029/2003JB002843.

596 Lichten, S. and J. Borders (1987). Strategies for High precision Global Positioning System Orbit
597 Determination, *J. Geophys. Res.*, 92, 12751-12762.

598 Li, Y.-G., and P. C. Leary (1990), Fault Zone Trapped Seismic Waves, *Bull. Seism. Soc. Am.*, 80,
599 5, 1245–1271.

600 McClusky, S., et al. (2000), GPS constraints on plate kinematics and dynamics in the eastern
601 Mediterranean and Caucasus, *J. Geophys. Res.*, 105, 5695-5719.

602 Melbourne, T. I., and F. H. Webb (2002), Precursory transient slip during the 2001 Mw = 8.4
603 Peru earthquake sequence from continuous GPS, *Geophys. Res. Lett.*, 29(21), 2032,
604 doi:10.1029/2002GL015533.

605 Miyazaki S., K. M. Larson, K. Choi, K. Hikima, K. Koketsu, P. Bodin, J. Haase, G. Emore, A.
606 Yamagiwa (2004), Modeling the rupture process of the 2003 September 25 Tokachi-Oki
607 (Hokkaido) earthquake using 1-Hz GPS data, *Geophys. Res. Lett.*, 31, L21603,
608 doi:10.1029/2004GL021457.

609 Paolucci, R. (2002). Amplification of earthquake ground motion by steep topographic
610 irregularities, *Earthquake Engng. Struct. Dyn.*, 31, 1831-1853.

611 Piatanesi, A., A. Cirella, P. Spudich, and M. Cocco (2007), A global search inversion for
612 earthquake kinematic rupture history: Application to the 2000 western Tottori, Japan earthquake, *J.*
613 *Geophys. Res.*, 112, B07314, doi:10.1029/2006JB004821.

614 Pino, N. A., and F. Di Luccio (2009), Source complexity of the 6 April 2009 L'Aquila (central
615 Italy) earthquake and its strongest aftershock revealed by elementary seismological analysis,
616 *Geophys. Res. Lett.*, 36, L23305, doi:10.1029/2009GL041331.

617 Press, W. H., S. A. Teukolsky, W. T. Vetterling and B. P. Flannery (1992), *Numerical Recipes in*
618 *C: The Art of Scientific Computing*, 2nd edn, Cambridge University Press, Cambridge.

619 Roberts, G. and A. M. Michetti, (2004), Spatial and temporal variations in growth rate along
620 active normal fault systems: an example from The Lazio Abruzzo Apennines, central Italy, *J.*
621 *Struct. Geol.,* 26**,** 339–376, doi:10.1016/S0191-8141(03)00103-2.

622 Ruegg, J. C., A. Rudloff, C. Vigny, R. Madariaga, J.B. de Chabalier, J. Campos, E. Kausel, S.
623 Barrientos, D. Dimitrov (2009), Interseismic strain accumulation measured by GPS in the seismic
624 gap between Constitución and Concepción in Chile, Physics of the Earth and Planetary Interiors,
625 175, 78–85

626 Smalley, R. Jr. (2009), High-rate GPS: How high do we need to go?, *Seism. Res. Lett.*, 80, 1054-
627 1061, doi:10.1785/gssrl.80.6.1054.

628 Trifunac, M. D. (1982), A note on rotational components of earthquake motions on ground
629 surface for incident body waves. *Soil Dynamics and Earthquake Engineering*, 1, 11–19.

630 Vigny, C., A. Socquet, J. A. Campos, D. Carrizo, J. Ruegg, M. Métois, S. Morvan, C. Aranda
631 (2010), The Maule Mw 8.8 earthquake and its consequences monitored by continuous and survey
632 mode GPS, *AGU Meeting of the Americas*, 8-12 August.

633 Yokota, Y., K. Koketsu, K. Hikima and S. Miyazaki (2009), Ability of 1-Hz GPS data to infer
634 the source process of a medium-sized earthquake: The case of the 2008 Iwate-Miyagi Nairiku,
635 Japan, earthquake, *Geophys. Res. Lett.*, 36, L12301, doi:10.1029/2009GL037799.

636 Wang, G., D. M. Boore, G. Tang and X. Zhou (2007), Comparisons of ground motions from
637 colocated and closely spaced one-sample-per-second global positioning system and accelerograph

638 recordings of the 2003 M 6.5 San Simeon, California, earthquake in the Parkfield region, *Bull.*
639 *Seism. Soc. Am.*, 97 (1B), 76-90, doi:10.1785/0120060053.

640 Wdowinski, S., Y. Bock, J. Zhang, P. Fung, and J. Genrich (1997). Southern California
641 permanent GPS geodetic array: spatial filtering of daily positions for estimating coseismic and
642 postseismic displacements induced by the 1992 Landers earthquake, *J. Geophys. Res.* **102,** 18,057.

643 Wessel, P., and W. H. F. Smith (1998), New, improved version of generic mapping tools
644 released, *Eos Trans. AGU*, *79*, 579.

645 Zumberge, J. F., M. B. Heflin, D. C. Jefferson, M. M. Watkins, & F. H. Webb (1997), Precise
646 point positioning for the efficient and robust analysis of GPS data from large networks, *J. Geophys.*
647 *Res.*, 102(B3), 5005-5018.
648

649

Tables Caption

Table 1. Mean co-seismic offsets of the GPS and SM sites (A), for each component (n, e, v), and relative 1-sigma uncertainties (σ) calculated before (^{b}) and after (^{a}) the mainshock (see text). Number of samples (N) used in each average and acquisition sampling rates (S), as well as site coordinates (Lat, Long) are also shown.

SITE	Lat (°)	Long (°)	A_n (cm)	σ_n^b (cm)	σ_n^a (cm)	A_e (cm)	σ_e^b (cm)	σ_e^a (cm)	A_v (cm)	σ_v^b (cm)	σ_v^a (cm)	N^b	N^a	S (Hz)
ROIO	42.327	13.386	-0.68	0.23	0.20	1.23	0.13	0.22	-10.31	0.24	0.30	50	50	10
CADO	42.293	13.483	4.24	0.28	0.36	-7.29	0.14	0.43	-15.21	0.34	0.38	50	50	10
INGP	42.382	13.316	-3.14	0.26	0.47	-0.26	0.10	0.66	-1.72	0.11	0.30	5	5	1
INFN	42.421	13.516	4.64	0.27	0.20	3.44	0.19	0.31	0.16	0.28	0.26	5	5	1
AQG	42.374	13.337	0.04	0.00	0.29	0.10	0.00	0.21	-0.52	0.00	0.10	1000	1000	200
AQK	42.345	13.401	0.15	0.01	0.44	-0.16	0.00	1.11	-15.57	0.00	0.23	1000	1000	200
AQU	42.354	13.402	-3.82	0.00	0.43	0.39	0.00	0.53	-15.02	0.00	0.20	500	500	100
GSA	42.421	13.519	4.06	0.01	0.08	5.57	0.00	0.24	1.15	0.00	0.11	1000	1000	200
GSG	42.460	13.550	2.21	0.00	0.08	3.23	0.00	0.07	0.34	0.01	0.14	1000	1000	200

657 **Table 2.** Parameters of power spectrum calculated for each GPS site solution and for each
658 component (n, e and v) in a 20 min time window: Site id, Sampling rate (S), spectral density levels
659 and relative standard errors at low (f_0=0.05 Hz, e_0) and high (Nyquist, e_1) frequencies. ([a]) indicates
660 preseismic solutions. For coseismic PSDs, spectral density maximum levels and relative frequency
661 value (e_p at *f*) are also shown. *GB06L and GB06N* indicate the 50-m-baseline 20-Hz solutions and
662 the 10-m-baseline 50-Hz solutions carried out by *Genrich and Bock* [2006] for LeicaGRX1200 and
663 NavCom instrumentation, respectively.

Site	S (Hz)	e_{0n} (cm^2/Hz)	e_{0e} (cm^2/Hz)	e_{0v} (cm^2/Hz)	e_{1n} (cm^2/Hz)	e_{1e} (cm^2/Hz)	e_{1v} (cm^2/Hz)	e_{pn} (cm^2/Hz at Hz)	e_{pe} (cm^2/Hz at Hz)	e_{pv} (cm^2/Hz at Hz)
ROIO	10	0.95 ± 0.14	0.45 ± 0.07	2.47 ± 0.36	0.003 ± 0.0005	0.002 ± 0.0002	0.009 ± 0.001	0.95 ± 0.14 at 0.04	0.45 ± 0.07 at 0.04	2.47 ± 0.4 at 0.04
ROIO	10[a]	0.93 ± 0.14	0.39 ± 0.06	1.10 ± 0.16	0.003 ± 0.0005	0.002 ± 0.0002	0.009 ± 0.001	-	-	-
ROIO	1	0.58 ± 0.07	0.20 ± 0.02	1.32 ± 0.15	0.08 ± 0.009	0.02 ± 0.003	0.11 ± 0.01	0.58 ± 0.07 at 0.06	0.24 ± 0.03 at 0.125	1.32 ± 0.2 at 0.06
CADO	10	1.22 ± 0.18	0.78 ± 0.11	2.50 ± 0.36	0.004 ± 0.0005	0.002 ± 0.0003	0.007 ± 0.001	1.22 ± 0.18 at 0.04	0.98 ± 0.14 at 0.7	2.63 ± 0.4 at 0.08
CADO	10[a]	0.97 ± 0.14	0.38 ± 0.06	1.02 ± 0.15	0.004 ± 0.0005	0.002 ± 0.0004	0.005 ± 0.0007	-	-	-
CADO	1	1.18 ± 0.14	0.62 ± 0.07	1.71 ± 0.20	0.05 ± 0.006	0.1 ± 0.01	0.17 ± 0.02	1.18 ± 0.14 at 0.06	2.35 ± 0.27 at 0.25	1.71 ± 0.2 at 0.06
INGP	1	0.25 ± 0.03	0.24 ± 0.03	0.57 ± 0.07	0.06 ± 0.007	0.13 ± 0.02	0.13 ± 0.02	0.25 ± 0.03 at 0.06	0.24 ± 0.03 at 0.06	0.57 ± 0.07 at 0.06
INGP	1[a]	0.34 ± 0.04	0.17 ± 0.02	0.78 ± 0.09	0.04 ± 0.004	0.03 ± 0.003	0.12 ± 0.01	-	-	-
INFN	1	0.52 ± 0.06	0.35 ± 0.04	0.78 ± 0.09	0.05 ± 0.006	0.04 ± 0.004	0.15 ± 0.02	0.52 ± 0.06 at 0.06	0.35 ± 0.04 at 0.06	0.78 ± 0.09 at 0.06
INFN	1[a]	0.40 ± 0.05	0.13 ± 0.02	0.79 ± 0.09	0.05 ± 0.005	0.01 ± 0.002	0.18 ± 0.02	-	-	-
GRO1	10	0.49 ± 0.04	0.42 ± 0.04	3.2 ± 0.3	0.0013 ± 0.0001	0.0011 ± 0.0001	0.008 ± 0.0007	-	-	-
GRO1	20	0.48 ± 0.04	0.41 ± 0.04	3.17 ± 0.3	0.0007 ± 6e-5	0.0006 ± 6e-5	0.0040 ± 0.0003	-	-	-
GB06L	20	-	-	-	0.0005	0.0004	0.0029	-	-	-
GB06N	50	-	-	-	0.0007	0.0004	0.0037	-	-	-

664

665 **Table 3.** Parameters of power spectrum calculated for GPS and SM solutions for each component (n, e and v) in a 45 s coseismic time window: Site
666 id; Sampling rate (S); spectral density levels and relative standard errors at low (f0=0.1Hz, e_0) and high (Nyquist, e_1) frequencies; spectral density
667 maximum levels and relative frequency value (e_p at *f*). (*) e_1 at 5Hz (and not at Nyquist frequency).

Site	Device	S (Hz)	e_{0n} (cm^2/Hz)	e_{0e} (cm^2/Hz)	e_{0v} (cm^2/Hz)	e_{1n} (cm^2/Hz)	e_{1e} (cm^2/Hz)	e_{1v} (cm^2/Hz)	e_{pn} (cm^2/Hz at Hz)	e_{pe} (cm^2/Hz at Hz)	e_{pv} (cm^2/Hz at Hz)
ROIO	GPS	10	2.2 ± 0.83	1.7 ± 0.66	1.7 ± 0.65	0.003 ± 0.0011	0.0014 ± 0.0005	0.012 ± 0.0047	2.2 ± 0.83 at 0.16	1.9 ± 0.73 at 0.31	1.7 ± 0.65 at 0.16
CADO	GPS	10	1.4 ± 0.52	4.6 ± 1.7	2.8 ± 1.1	0.018 ± 0.007	0.011 ± 0.0043	0.011 ± 0.004	5.8 ± 2.2 at 0.78	21 ± 7.9 at 0.78	2.8 ± 1.1 at 0.16
AQK	SM	200	3.1 ± 1	0.85 ± 0.29	2.8 ± 0.93	6.9e-05* ± 2.3e-05	4.3e-05* ± 1.5e-05	1.4e-4* ± 4.7e-05	5 ± 1.7 at 0.39	5.4 ± 1.8 at 0.59	2.8 ± 0.93 at 0.2
AQU	SM	100	1.5 ± 0.49	0.83 ± 0.28	5.5 ± 1.9	1.6e-5* ± 5.4e-6	6.1e-6* ± 2.1e-6	5.3e-5* ± 1.8e-5	1.8 ± 0.62 at 0.39	1 ± 0.35 at 0.39	5.5 ± 1.9 at 0.2
INGP	GPS	1	0.58 ± 0.17	2.6 ± 0.76	0.29 ± 0.087	0.64 ± 0.19	3.3 ± 0.98	0.43 ± 0.13	0.64 ± 0.19 at 0.5	3.3 ± 0.98 at 0.5	0.43 ± 0.1 at 0.5
AQG	SM	200	0.2 ± 0.067	1.5 ± 0.5	0.1 ± 0.034	1.6e-4* ± 5.4e-05	1e-4* ± 3.5e-05	1.4e-05* ± 4.7e-06	0.3 ± 0.1 at 1.2	1.6 ± 0.55 at 0.39	0.17 ± 0.06 at 0.39
INFN	GPS	1	0.38 ± 0.11	0.46 ± 0.13	0.2 ± 0.06	0.38 ± 0.11	0.5 ± 0.15	0.23 ± 0.068	0.38 ± 0.11 at 0.25	0.5 ± 0.15 at 0.5	0.23 ± 0.07 at 0.5
GSA	SM	200	0.65 ± 0.22	0.55 ± 0.19	0.33 ± 0.11	4.7e-05* ± 1.6e-05	3e-05* ± 1e-05	1e-05* ± 3.4e-06	0.65 ± 0.22 at 0.2	0.57 ± 0.19 at 0.39	0.33 ± 0.11 at 0.2
GSG	SM	200	0.43 ± 0.14	0.3 ± 0.1	0.35 ± 0.12	5.6e-07* ± 1.9e-07	2.9e-07* ± 1e-07	4.2e-07* ± 1.4e-07	0.43 ± 0.14 at 0.2	0.3 ± 0.1 at 0.2	0.35 ± 0.12 at 0.2

668 **Figures Caption**

669

670 **Figure 1: Coseismic displacements of the 2009 April 6th Mw 6.3 L'Aquila earthquake (grey**
671 **star) for the 10-Hz GPS sites (black vectors) and the 1-Hz CGPS sites (white**
672 **vectors) determined by the VHRGPS data analysis, as well as for the SM sites (grey**
673 **vectors) determined by the double-integration procedure. The grey box represents**
674 **the surface projection of the fault model proposed by *Cirella et al.* [2009] and the**
675 **ticked line represents the intersection of the fault with the surface. The map in the**
676 **lower-left corner shows the observed VHRGPS and SM vertical displacements.**
677 **Black lines are active faults from *Boncio et al.* [2004], *Roberts and Michetti* [2004]**
678 **and *Galli et al.* [2008].**

679 **Figure 2: 10-Hz (solid lines) and 1-Hz (dashed lines) dynamic displacements for the GPS sites:**
680 **ROIO (a), CADO (b), INGP (c) and INFN (d). The horizontal axis denotes seconds**
681 **from 2009 April 6th, 01:32:35 UTC, and the vertical scale denotes displacement (in**
682 **centimeters). Vertical thin line indicates the L'Aquila earthquake time occurrence**
683 **(01:32:40.78 [*Chiarabba et al.,* 2009]). Co-seismic offsets and their 99% confidence**
684 **level from *Cheloni et al.* [2010] (circles) and *Anzidei et al.* [2009] (triangles) are also**
685 **shown and arbitrarily plotted at epochs 28 s and 29 s, respectively. Red, green and**
686 **blue colors indicate North, East and Up components, respectively.**

687 **Figure 3: PSD functions, calculated in a 20 min time window, for the 10-Hz (thick solid lines)**
688 **and the 1-Hz (dashed lines) coseismic solutions and PSD functions for the 10-Hz**
689 **pre-seismic solutions (thin solid lines): a) ROIO; b) CADO; c) INGP; d) INFN. Red,**
690 **green and blue colors indicate North, East and Up components, respectively. ROIO**

and CADO have the same horizontal and vertical scales. INGP and INFN have the same horizontal and vertical scales, but not the same as ROIO and CADO.

Figure 4: PSD functions, calculated in a 1 hour time window (day 319, 2009), for the 20-Hz (thin lines) and the 10-Hz (thick lines) solutions for a RING CGPS site (GRO1). Red, green and blue colours indicate North, East and Up components, respectively.

Figure 5: a) Comparison of position time series between the 10-Hz GPS CADO (red) and the closer accelerometers AQK (blue) and AQU (green). b) Comparison of position time series between the 10-Hz GPS ROIO (purple) and the closer accelerometers AQK (blue) and AQU (green). c) Comparison of position time series between the 1-Hz GPS (INGP, purple, and INFN, red) and the closer accelerometers (AQG, black, and GSA, green, and GSG, blue, respectively). For each component, the comparisons INGP-AQG and INFN-GSA-GSG are vertically shifted for clarity. The horizontal axis denotes seconds from 2009 April 6th 01:32:35 UTC, and the vertical scale denotes displacement (in centimeters). d) Comparison of PSD functions between 10-Hz GPS solutions (ROIO, purple, and CADO, red), and the closer SM (AQK, blue, and AQU, green).

Figure 6: Kinematic rupture model projected on the Earth surface (a) and in the fault plane geometry (b). Colours on the fault planes indicate the slip distribution. Black triangles indicate the GPS and strong motion sites. Red vectors represent observed GPS static offsets, whereas the blue vectors represent the modelled ones.

Figure 7: a) Comparison of recorded strong motions and GPS velocities (blue lines) with synthetic waveforms computed from the kinematic rupture model (red lines). The amplitude of the waveforms is in cm/s. b) Fit for the four high-rate dynamic GPS

stations expressed in displacement for East, North and Vertical components, respectively. Blue, red and green traces displays the synthetic, observed signal (modelled between 0.02 and 0.5 Hz), and the original (no filtered) displacement, respectively. Numbers with each trace are peak amplitude of the observed waveforms in cm/s (a) and cm (b).

Figure SM1: Different positions estimations for CADO 10-Hz co-seismic recording: comparison between the white noise solution (run1) and a tight random walk solution (run2). Stochastic parameters used for position estimations are shown in Table SM1.

Figure SM2: Residuals between the unfiltered 10-Hz time series and the one filtered by applying the modified sidereal filtering: CADO (thick lines); ROIO (dashed lines). Red, green and blue colours indicate North, East and Up components, respectively.

Figure SM3: a) Kinematic rupture model in the fault plane (average model from ensemble inference) of the 2009 L'Aquila earthquake. Left, middle and right panels show total slip, rise time and peak slip velocity distributions, respectively. The rupture time is shown by contour lines (in seconds); the black arrows displayed in left panel represent the slip vector. b) Rupture history of the 2009 L'Aquila earthquake as obtained by *Cirella et al.* [2009].

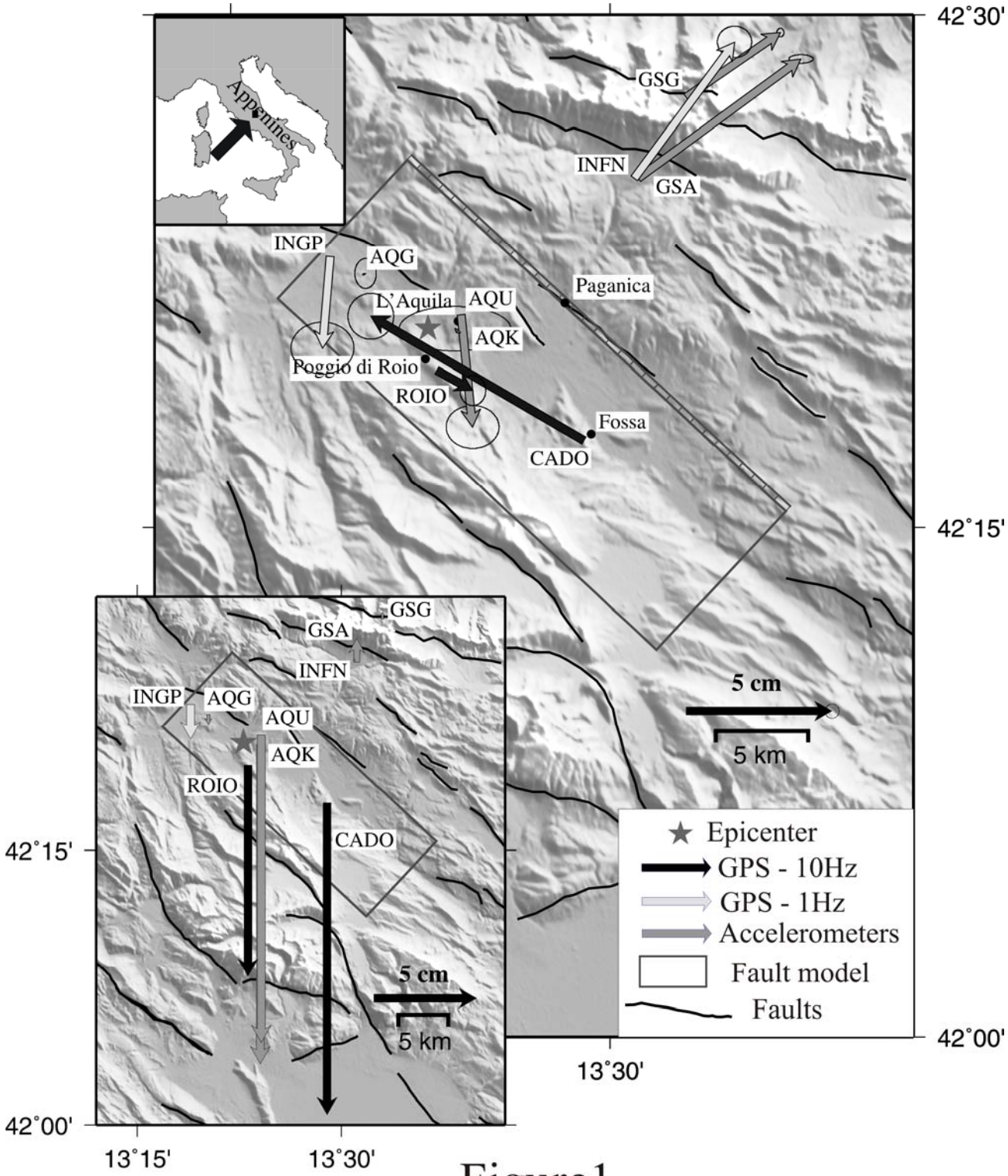

Figure1

733

734

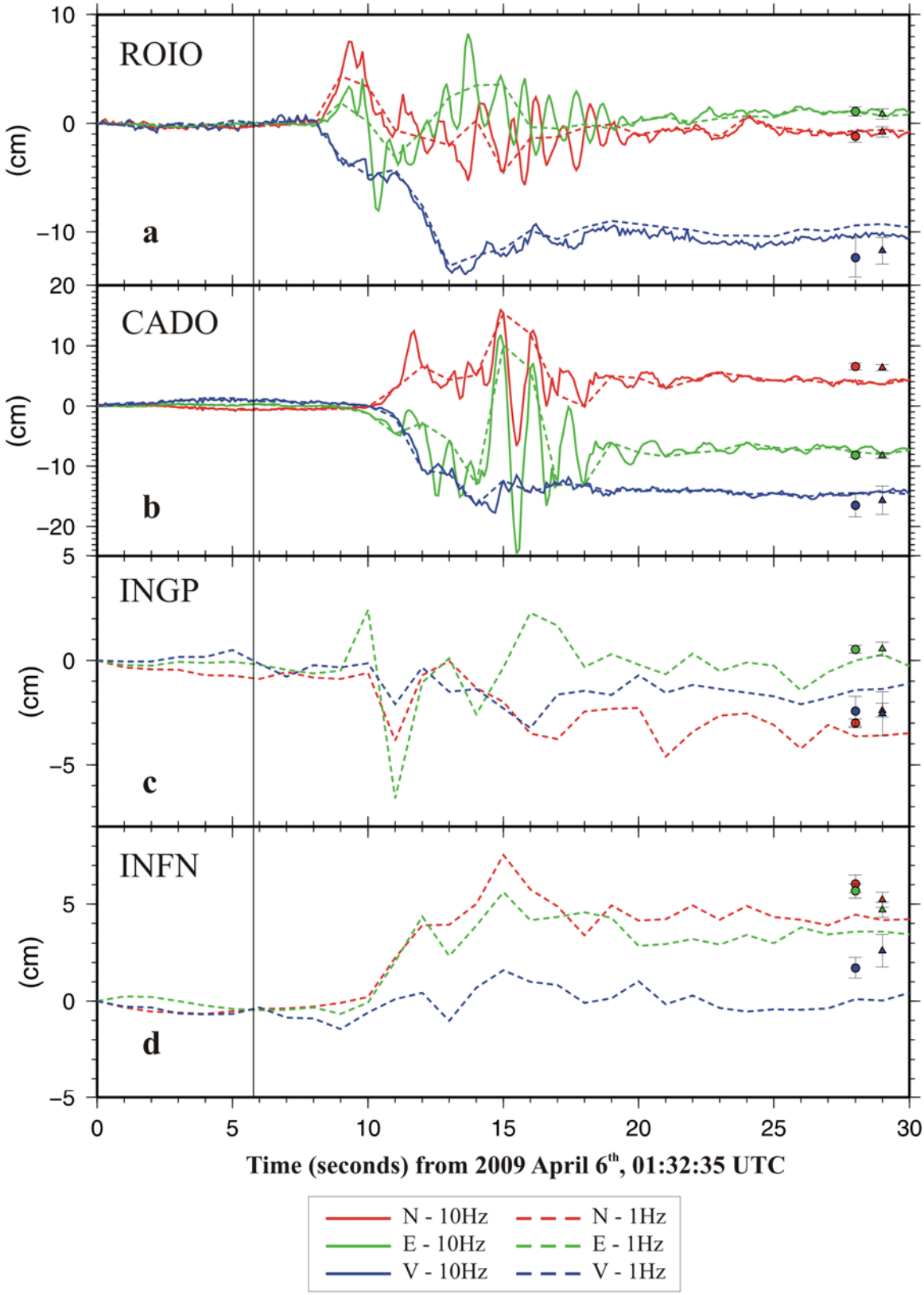

Figure2

735

736

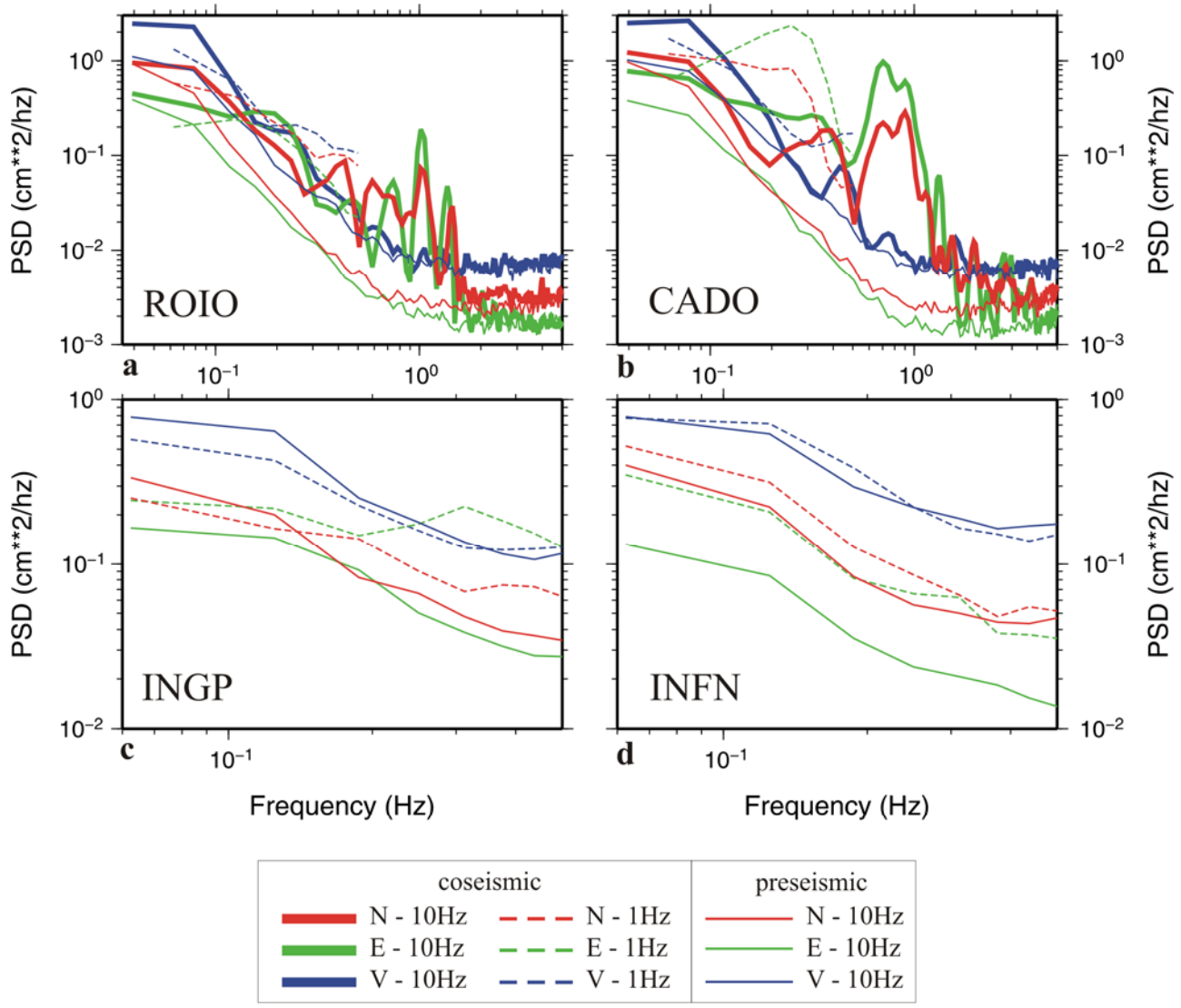

Figure3

737

738

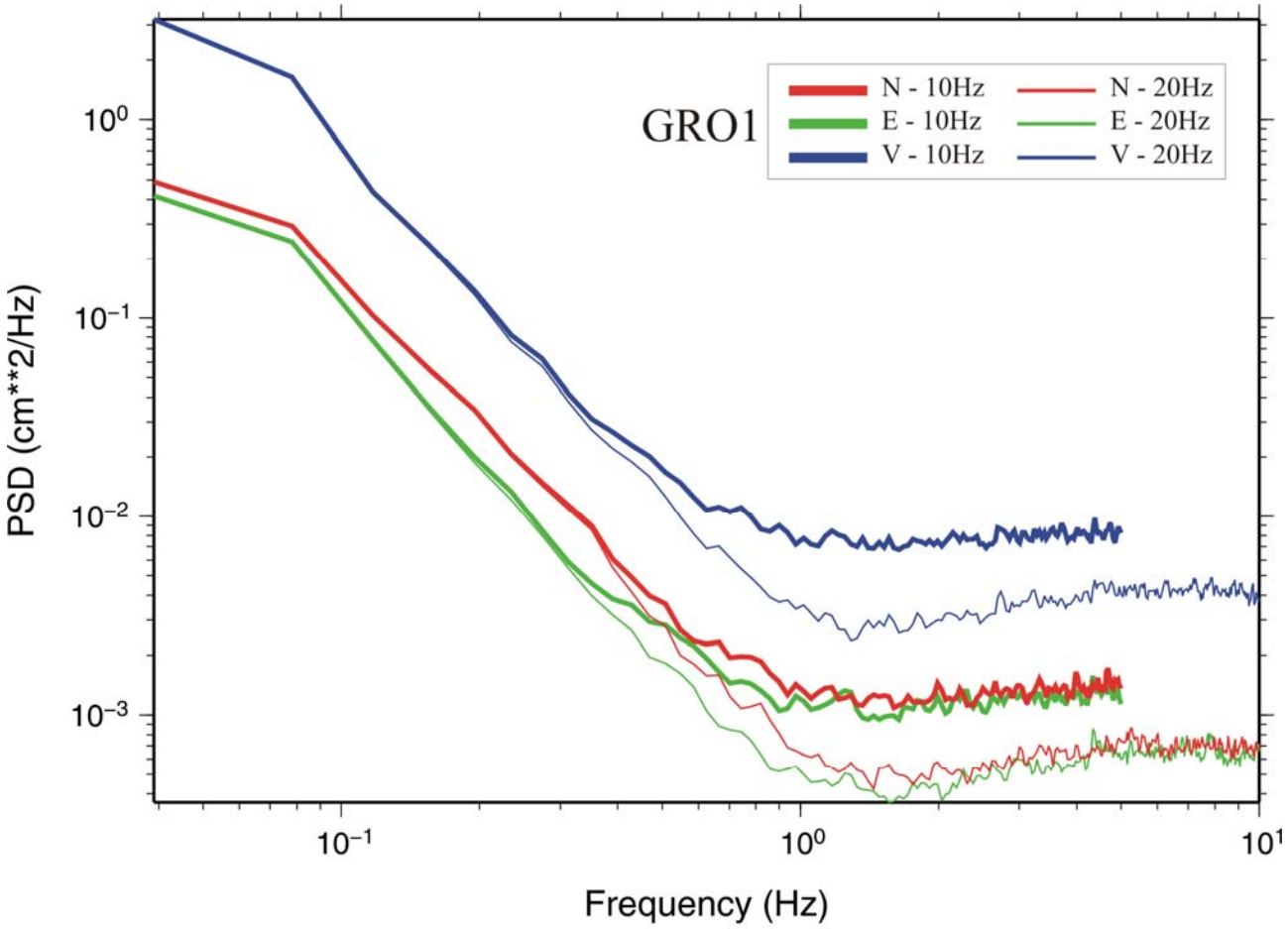

Figure4

739

740

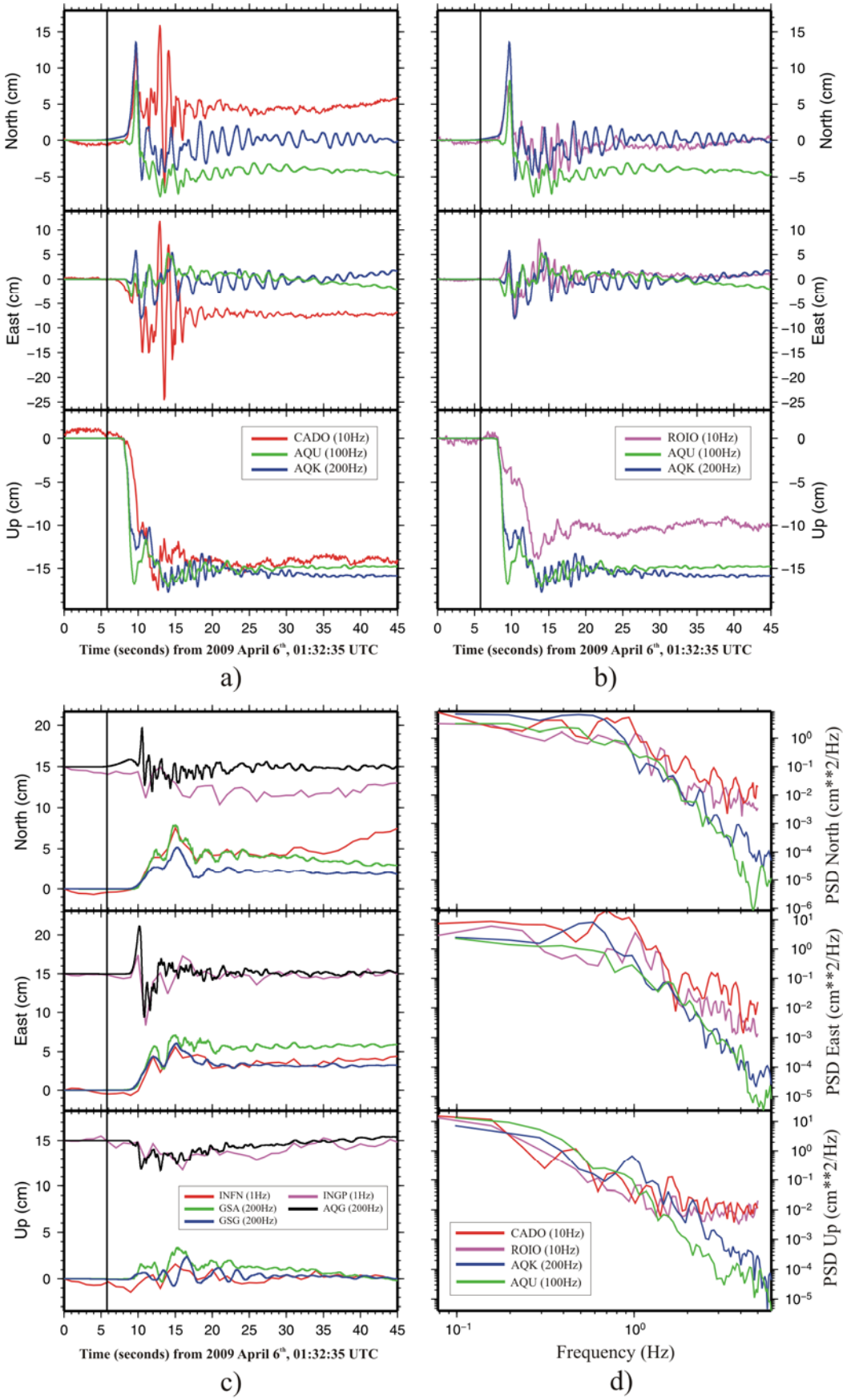
North (cm)
East (cm)
Up (cm)
CADO (10Hz)
AQU (100Hz)
AQK (200Hz)
Time (seconds) from 2009 April 6th, 01:32:35 UTC
a)
ROIO (10Hz)
AQU (100Hz)
AQK (200Hz)
Time (seconds) from 2009 April 6th, 01:32:35 UTC
b)
INFN (1Hz)
INGP (1Hz)
GSA (200Hz)
AQG (200Hz)
GSG (200Hz)
Time (seconds) from 2009 April 6th, 01:32:35 UTC
c)
PSD North (cm**2/Hz)
PSD East (cm**2/Hz)
PSD Up (cm**2/Hz)
CADO (10Hz)
ROIO (10Hz)
AQK (200Hz)
AQU (100Hz)
Frequency (Hz)
d)

Figure 5

741

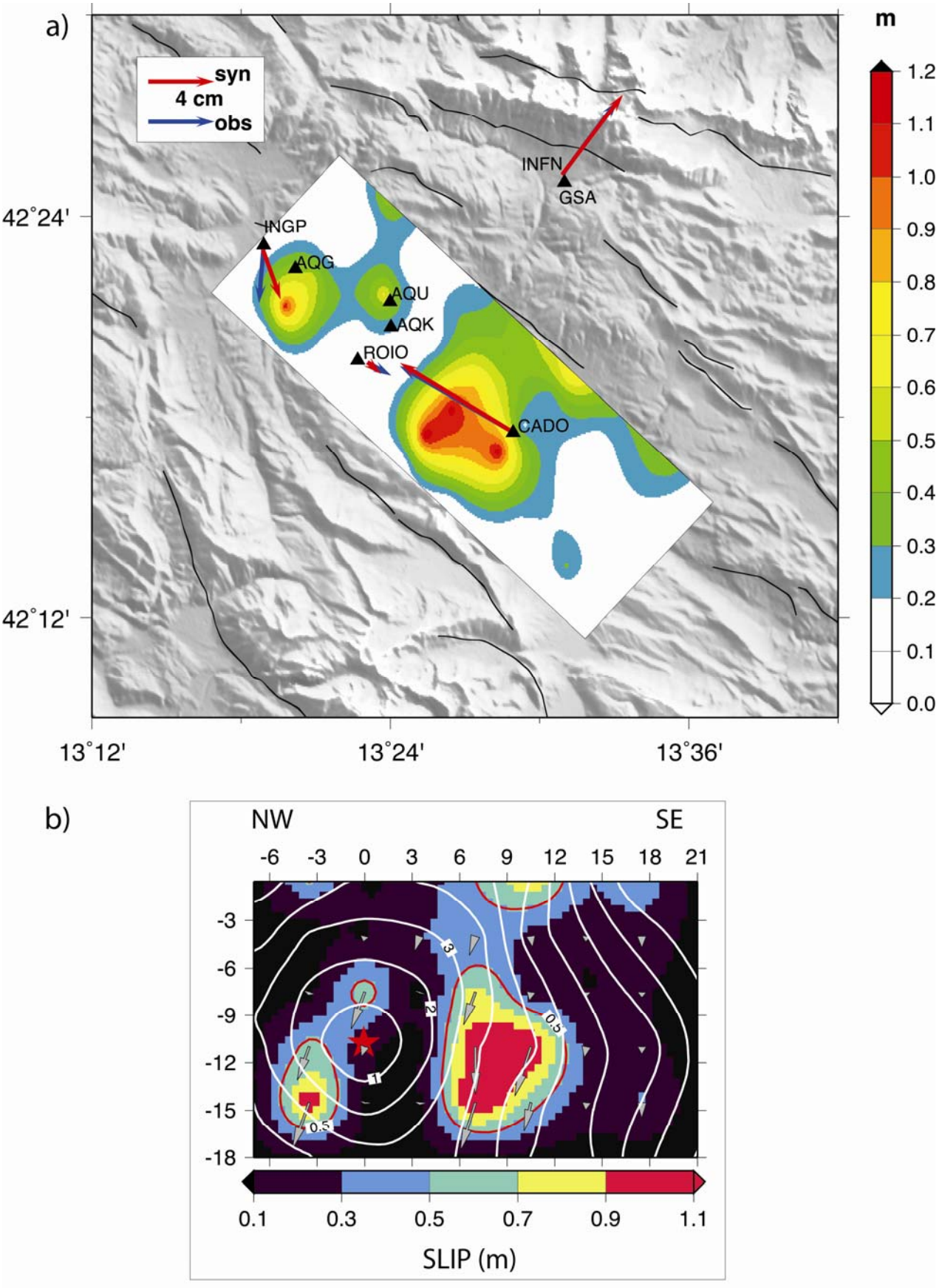
a)
syn
4 cm
obs
INFN
GSA
INGP
AQG
AQU
AQK
ROIO
CADO
42°24'
42°12'
13°12'
13°24'
13°36'
m
1.2
1.1
1.0
0.9
0.8
0.7
0.6
0.5
0.4
0.3
0.2
0.1
0.0
b)
NW
SE
-6 -3 0 3 6 9 12 15 18 21
-3
-6
-9
-12
-15
-18
3
2
1
0.5
0.5
0.1 0.3 0.5 0.7 0.9 1.1
SLIP (m)

Figure 6

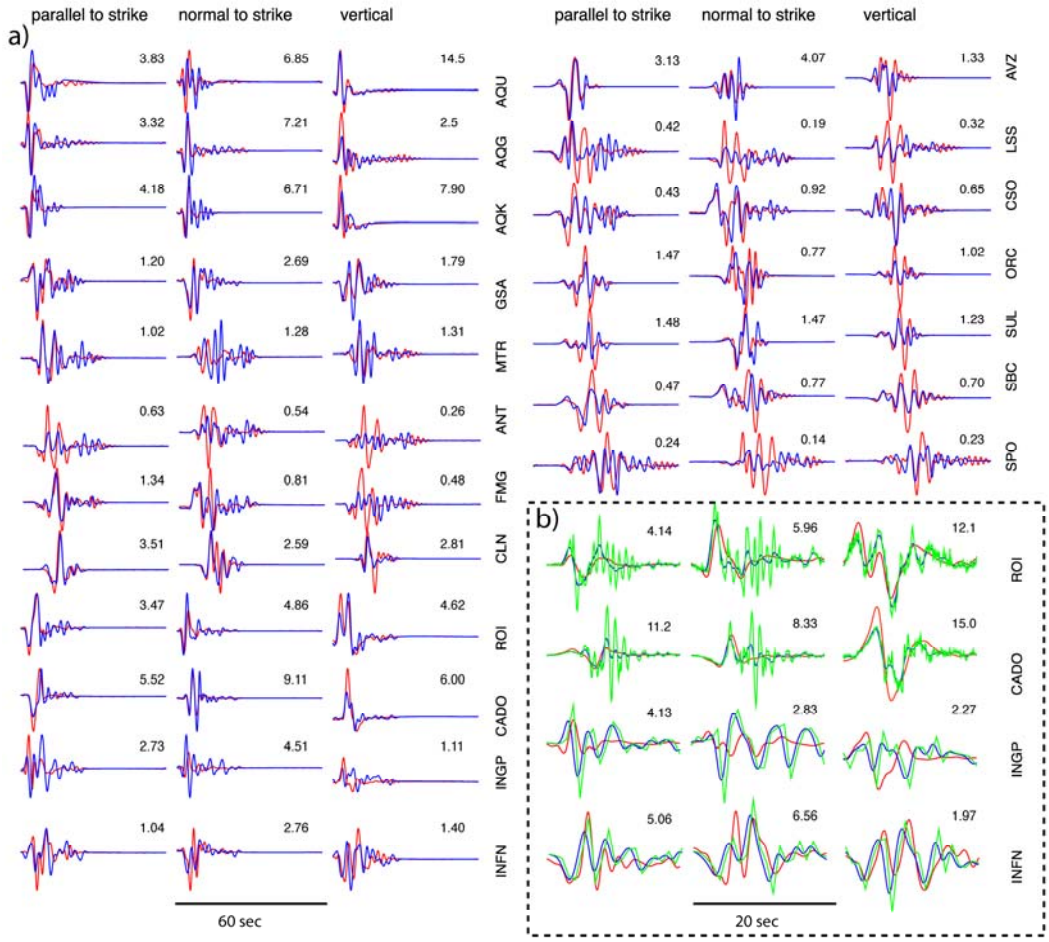

743 Figure 7

744

Auxiliary Material Submission for Paper 2010JB007834

10 Hz GPS seismology for moderate magnitude earthquakes: the case of the Mw 6.3 L'Aquila (Central Italy) event

A. Avallone1, M. Marzario1, A. Cirella2, A. Piatanesi2, A. Rovelli2, C. Di Alessandro3, E. D'Anastasio1, N. D'Agostino1, R. Giuliani4, and M. Mattone4.

1. Istituto Nazionale di Geofisica e Vulcanologia, Centro Nazionale Terremoti, Via di Vigna Murata 605, I-00143, Roma, Italy.

2. Istituto Nazionale di Geofisica e Vulcanologia, sezione di Roma1,
Via di Vigna Murata 605, I-00143, Roma, Italy.

3. Pacific Earthquake Engineering Research Center (PEER), University of California, Berkeley, 325 Davis Hall, Mail Code 1792, Berkeley, CA 94720-1792, USA.

4. Dipartimento della Protezione Civile, Ufficio Rischio Sismico,
Via Vitorchiano 4, I-00189, Roma, Italy.

Description of the auxiliary comparisons.

This data set contains three figures showing different type of comparisons. The first two figures deal with comparisons between differently estimated 10-HZ GPS solutions, whereas the third figure concerns the comparison between two different kinematic rupture models for the L'Aquila earthquake. We tested both white noise and random walk noise to estimate site positions epoch-by-epoch (2010jb007834-ts01.txt). Details of the other aspects of the high-rate GPS data analysis (troposphere delay estimation, orbits and clocks used, etc.) are given in the main text. For the white noise, we set the a-priori standard deviation of position to 1 m. For the random-walk noise, we set the a-priori standard deviation of position to 1 m and the steady-state standard deviation to about 1.6 cm. The comparison, shown in the figure 2010jb007834-fs01.tif, points out the in a 30 s time window, the two solutions almost overlap. Aim of the second comparison is to quantify the contribution of the multipath in this 30-s-spanning HRGPS signal. To determine sidereal contribution, we followed the method described by Choi et al. [2004]. For both the HRGPS sites (ROIO and CADO), the residuals between unfiltered and filtered signals show a low frequency trend (2010jb007834-fs02.tif) and are well within the RMS of the HRGPS time series (1.3, 0.6 and 3 cm for north, east and vertical components, respectively). This suggests that sidereal filtering does not significantly affect the high

frequency coseismic dynamic displacements. The last figure (2010jb007834-fs03.tif) shows the comparison between the kinematic rupture model obtained in this study and the one obtained in Cirella et al. [2009]. The two models are in agreement: the slip, rise time and peak slip velocity distributions are almost the same as Cirella et al. [2009], with the exception of a patch of slip located below the hypocenter, due to aliased (and thus not-reliable) INGP solution.

1. 2010jb007834-ts01.txt (Table SM1): Parameters defining the stochastic determination of the GPS stations positions [Lichten and Borders, 1987]: a-priori standard deviation (apsig), steady state standard deviation (sigp), sampling rate (sdelt) and stochastic estimation type (smtau).

1. 2010jb007834-fs01.tif (Figure SM1): Different positions estimations for CADO 10-Hz co-seismic recording: comparison between the white noise solution (run1) and a tight random walk solution (run2). Stochastic parameters used for position estimations are
shown in Table SM1.

2. 2010jb007834-fs02.tif (Figure SM2): Residuals between the unfiltered 10-Hz time series and the one filtered by applying the modified sidereal filtering: CADO (thick lines); ROIO (dashed lines). Red, green and blue colours indicate North, East and Up components, respectively.

3. 2010jb007834-fs03.tif (Figure SM3): a) Kinematic rupture model in the fault plane (average model from ensemble inference) of the 2009 L'Aquila earthquake. Left, middle and right panels show total slip, rise time and peak slip velocity distributions, respectively. The rupture time is shown by contour lines (in seconds); the black arrows
displayed in left panel represent the slip vector. b) Rupture history of the 2009 L'Aquila earthquake as obtained by Cirella et al. (2009).

References

Choi, K., A. Bilich, K. M. Larson, and P. Axelrad (2004), Modified sidereal filtering: Implications for high-rate GPS positioning Geophys. Res. Lett., Vol. 31, No.22, L22608, doi 10.1029/2004GL021621.

Cirella, A., A. Piatanesi, M. Cocco, E. Tinti, L. Scognamiglio, A. Michelini, A. Lomax and E. Boschi (2009), Rupture history of the 2009 L'Aquila (Italy) earthquake from non-linear joint inversion of strong motion and GPS data, Geophys. Res. Lett., 36, L19304, doi:10.1029/2009GL039795.

Lichten, S. and J. Borders (1987). Strategies for High precision Global Positioning System Orbit Determination, J. Geophys. Res., 92, 12751-12762.

Table SM1 : Parameters defining the stochastic determination of the GPS stations positions [Lichten and Borders, 1987]: a-priori standard deviation (apsig), steady state standard deviation (sigp), sampling rate (sdelt) and stochastic estimation type (smtau).

run	apsig (km)	sigp (km or km/s-1/2)	sdelt (s)	smtau
1	1.00E-03	1.00E-03	0.1	WHITENOISE
2	1.00E-03	5.00E-05	0.1	RANDOM WALK (tight)

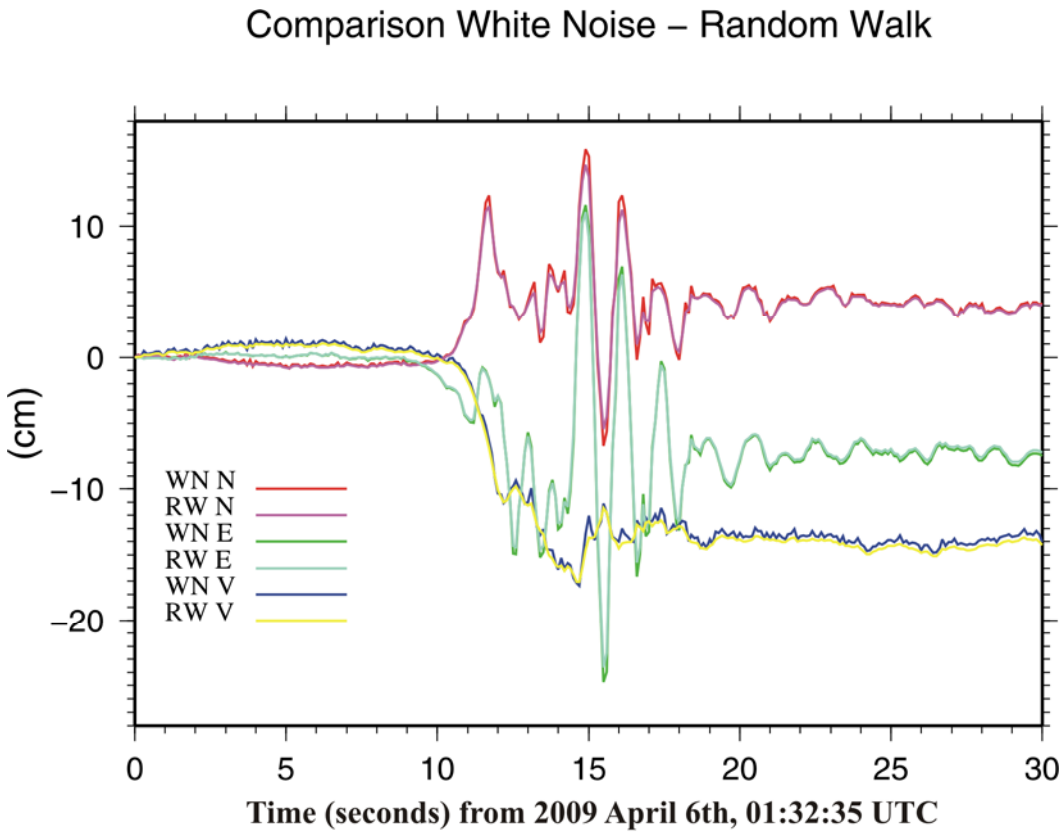

FigureSM1

861

862

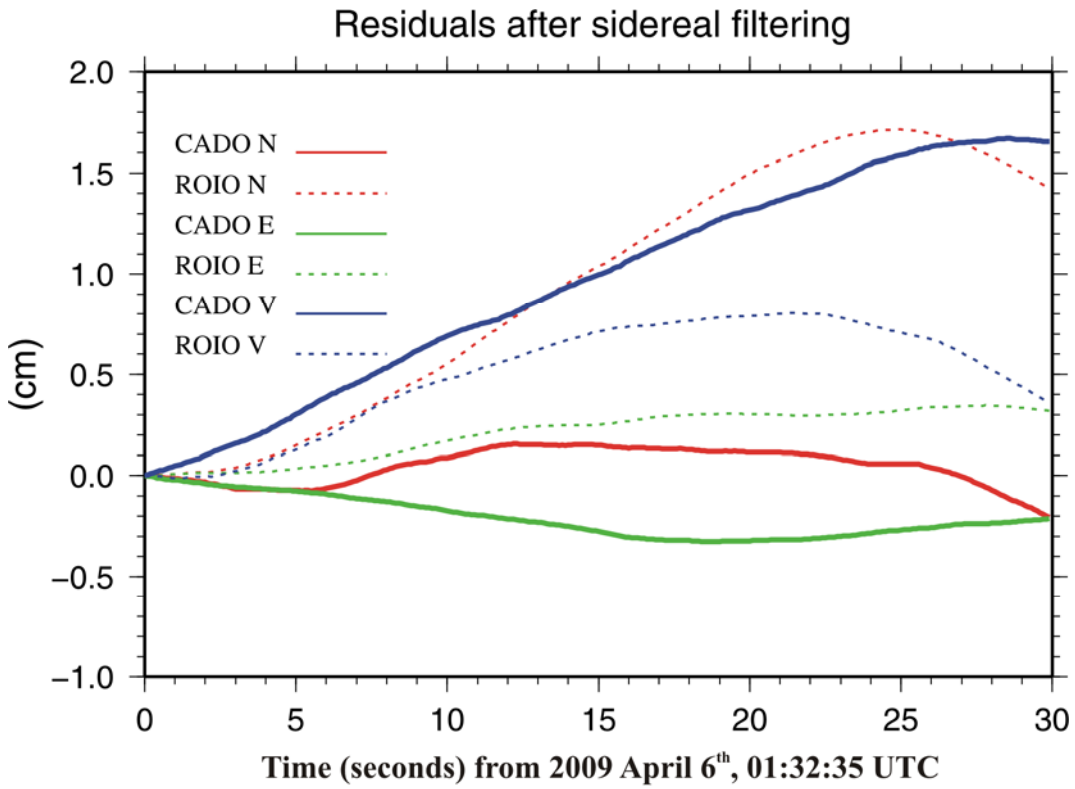

FigureSM2

863

864

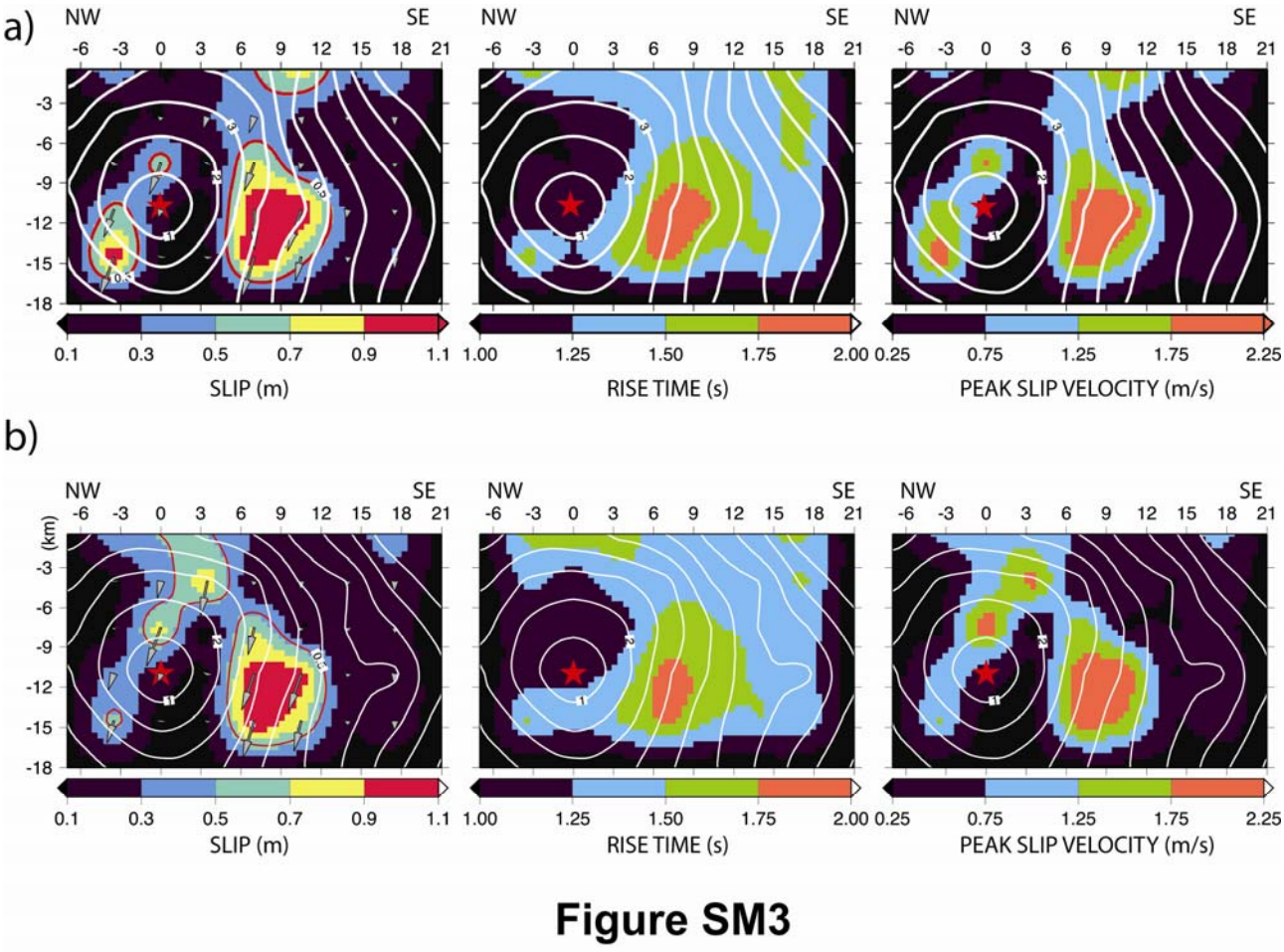
a)
NW
SE
-6 -3 0 3 6 9 12 15 18 21
-3
-6
-9
-12
-15
-18
0.1 0.3 0.5 0.7 0.9 1.1
SLIP (m)
1.00 1.25 1.50 1.75 2.00
RISE TIME (s)
0.25 0.75 1.25 1.75 2.25
PEAK SLIP VELOCITY (m/s)
b)
(km)

Figure SM3